ISSN 2096-7071 (Print)
ISSN 2097-3101 (Online)
CN 10-1629/R1

CHINA CDC WEEKLY

Vol. 8 No. 40 Oct. 2, 2026

CCDC weekly

中国疾病预防控制中心周报(英文)

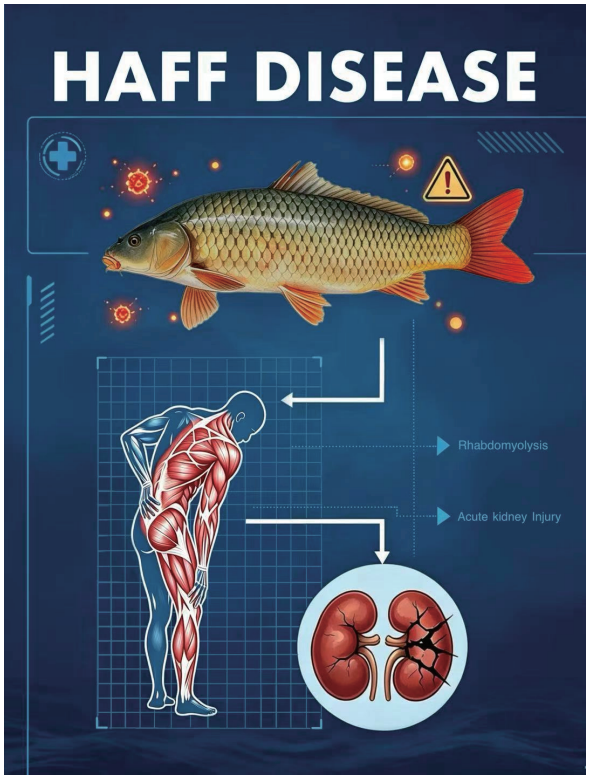

Vital Surveillances

Epidemiological and Genetic Characterization of Human Metapneumovirus in Children — Tianjin, China, 2012–2024 1225

Methods and Applications

Safety of PCV13 with Different Carrier Proteins (CRM197, TT, and TT/DT) — Jiangsu Province, China, 2022–2024 1234

Preplanned Studies

Genomic Epidemiology and Antimicrobial Susceptibility of Human Brucellosis — Shenzhen City, Guangdong Province, China, 2005–2024 1242

Outbreak Reports

Early Detection and Response to the First Imported Case of Zika Virus Disease — Hainan Province, China, 2025 1252

A Cluster of Haff Disease Associated with Consumption of *Cyprinus carpio rubrofuscus* — Heyuan City, Guangdong Province, China, 2026 1257

Notifiable Infectious Diseases Reports

Reported Cases and Deaths of National Notifiable Infectious Diseases — China, July 2026 1261

ISSN 2096-7071
40>
9 772096 707262

China CDC Weekly

Editorial Board

Honorary Editor-in-Chief Hongbing Shen

Founding Editor-in-Chief George F. Gao

Advisory Board Member Jianguo Xu Liming Li Yu Wang Gabriel M Leung Zijian Feng

Editor-in-Chief Jianwei Wang

Deputy Editor-in-Chief

Zhuo Chen (USA) Zhibin Hu Qun Li Zhengliang Li Xiaoming Shi Yan Sun
Changjun Wang Tangchun Wu Yongning Wu Ningshao Xia Chihong Zhao

Editorial Board Member

Jianping Cao Guobing Chen Xi Chen (USA) Gong Cheng Gangqiang Ding
Xiaoping Dong Pei Gao Xin Guo Jun Han Mengjie Han
Weidong Hao Na He Yuping He Guoqing Hu Cunrui Huang
John S. Ji (USA) Na Jia Weihua Jia Zhongwei Jia Biao Kan
Haidong Kan Jianqiang Lai Lance Rodewald (USA) Ni Li Shizhu Li
Ying Li Zhenjun Li Zhongjie Li Geyu Liang Yuan Lin
Aidong Liu Min Liu Qiyong Liu Qingjie Liu Yawen Liu
Jinxing Lu Xiangfeng Lu David LYE Chien Boon (Singapore) Fan Lyu
Jun Lyu Huilai Ma Jiaqi Ma Chen Mao Xiaoping Miao
An Pan Jie Pan Lili Ren Guoqing Shi Yuelong Shu
Chengye Sun Quanfu Sun Xin Sun Hua Wang Huaqing Wang
Hui Wang Jianming Wang Junling Wang Lin Wang Tong Wang
Shenghui Wu (USA) Min Xia Lin Xiao Dongqun Xu Hongyan Yao
Guojing Yang Zundong Yin Dianke Yu Hongjie Yu Siyan Zhan
Jianzhong Zhang Jun Zhang Liubo Zhang Tao Zhang Yanping Zhang
Wei Zhao Yanlin Zhao Maigeng Zhou Xiaonong Zhou Yongqun Zhu
Guihua Zhuang

Editorial Office

Directing Editor Chihong Zhao

Managing Editor Yu Chen

Senior Scientific Editors

Xuejun Ma Daxin Ni Ning Wang Wenwu Yin Shicheng Yu Jianzhong Zhang Qian Zhu

Scientific Editors

Weihong Chen Jie Dong Tao Jiang Dongmin Li Xudong Li Nankun Liu
Liwei Shi Meng Wang Zhihui Wang Qi Yang Qing Yue Lijie Zhang
Ying Zhang Lishu Zheng

Editor in Charge Meng Wang

Cover Image: credited from the designer Jiaying Wang.

Vital Surveillances

Epidemiological and Genetic Characterization of Human Metapneumovirus in Children — Tianjin, China, 2012–2024

Mingkun Wu[1,2,&]; Rui Li[3,&]; Liru Guo[1,2]; Mei Kong[1,2]; Peng Zhang[1,2]; Xiaoyan Li[1,2,4,#]

ABSTRACT

Introduction: Human metapneumovirus (HMPV) is a common cause of acute respiratory tract infections (ARTIs) in children. This study characterized the epidemiological patterns of pediatric HMPV infection in Tianjin from 2012 to 2024 and analyzed the genetic features of circulating strains to inform prevention and control strategies.

Methods: Epidemiological data collected from 2012 to 2024 were retrospectively analyzed to describe the seasonality and age distribution of pediatric HMPV infection. Novel primers were designed for whole-genome sequencing, and circulating HMPV strains were characterized by subtype, recombination signals, amino acid substitutions, and glycosylation sites.

Results: Pediatric HMPV infection in Tianjin showed seasonal and age-related patterns. The dominant type alternated between HMPV-A and HMPV-B every 1–3 years. Four major subtypes, A2b, A2c, B1, and B2, were detected, and A2c predominated in recent years. Genetic and molecular analyses identified recombination signals in several sequences, as well as amino acid substitutions and glycosylation sites.

Conclusion: This study characterized the epidemiological patterns of pediatric HMPV infection in Tianjin from 2012 to 2024. The newly designed primers supported whole-genome sequencing and analyses of viral genetic variation and recombination. These findings provide epidemiological and genomic evidence to inform HMPV prevention and control.

Acute respiratory tract infections (ARTIs) cause substantial morbidity and mortality and pose a global public health threat (*1*). Human metapneumovirus (HMPV), a previously unrecognized ARTI-associated virus, was first isolated in the Netherlands in 2001 from 28 infants with respiratory tract infections (*2*). Its genome is approximately 13 kb and contains eight genes encoding nine proteins (*3*). Based on the genetic characteristics of the F and G genes, HMPV is classified into four subtypes (A1, A2, B1, and B2) and further into the A1, A2a, A2b, A2c, B1, and B2 lineages (*4*). Subtypes reported to circulate in China are A2b, B1, and B2 (*5*).

HMPV infection can cause mild to severe upper and lower respiratory tract disease, and children younger than 5 years are particularly susceptible (*6*). Nearly all children experience one or more infections by 5 years of age, but infection does not induce persistent immunity (*7*). HMPV is an important public health concern, particularly in low- and middle-income countries, where it imposes a substantial annual healthcare burden (*8*).

This study retrospectively analyzed epidemiological data from 8,325 pediatric outpatients with influenza-like illness (ILI) in Tianjin during 2012–2024. Phylogenetic and molecular analyses characterized HMPV genomic variation, including recombination signals, amino acid substitutions, and glycosylation sites. The findings provide baseline etiological evidence for HMPV vaccine and antiviral drug development.

MATERIALS AND METHODS

Participants and Samples

Throat swabs were collected weekly during 2012–2024 from outpatients with ILI at Tianjin Children's Hospital, yielding 8,325 specimens; all participants were younger than 18 years. ILI was defined as fever (body temperature ≥38.0 °C) accompanied by cough or sore throat. HMPV was detected and genotyped for subgroups A/B by quantitative reverse-transcription polymerase chain reaction (qRT-PCR) according to the product instructions using TransScript® Probe One-Step qRT-PCR SuperMix (TransGen Biotech, Beijing, China). The HMPV primers (F: CATATAAGCATGCTATAT

Copyright © 2026 by Chinese Center for Disease Control and Prevention

TAAAAGAGTCTCA, R: CCTATTTCTGCAGC ATATTTGTAATCAG) and subtype-specific primers (F: TGATGCRCTCAAAAGATACCC, R: ACRAAYA AACTTTCTGCTTTGC), FAM-labelled HMPV probe (FAM-CAACHGCAGTGACACCCTCATCA TTGCA-TAMAR), FAM-labelled HMPV-A probe (FAM-TGGCAAAGCATTAGGCTCATCCTCT-BHQ1) and HEX-labelled HMPV-B probe (HEX-GCTTTAGGCTCATCTTCAACAGGRA-BHQ1), were obtained from GENEWIZ Biotech (Suzhou, China). A cycle threshold (Ct) <36 with an exponential amplification curve was considered positive.

HMPV Whole-Genome Sequencing and Genome Assembly

In total, 389 complete HMPV sequences were downloaded from the National Center for Biotechnology Information (NCBI). Nine primer pairs were designed using Geneious Prime (version 2023.0.4; Dotmatics, Boston, MA, United States) (Supplementary Table S1, available at https://weekly.chinacdc.cn/). Amplification products were confirmed by agarose gel electrophoresis (Supplementary Figure S1, available at https://weekly.chinacdc.cn/). Amplification was performed using Platinum™ SuperFi™ PCR Master Mix (Invitrogen, United States); protocols are presented in Supplementary Tables S2–S3 (available at https://weekly.chinacdc.cn/). HMPV-positive samples with Ct values ≤35 underwent whole-genome sequencing using these primers. DNA libraries were prepared with the Nextera XT DNA Library Preparation Kit and sequenced paired-end on the NextSeq 2000 System (Illumina, Inc., United States).

Sequencing Data Processing

Low-quality reads were filtered out, reads were mapped, and consensus sequences were extracted using CLC Genomics Workbench (version 21.0.4; Qiagen, Hilden, Germany). In total, 79 sequences had coverage ≥90%, of which 40 were complete genomes with lengths of 13,045–13,390 nucleotides (nt).

Phylogenetic Analysis and Genetic Variation of HMPV Strains

HMPV types were assigned using Nextclade (version 3.21.0; Nextstrain Team, Basel, Switzerland) (*9*). Recombination signals were assessed using Recombination Detection Program version 4 (RDP4) (version 4.101; University of Cape Town, Cape Town, South Africa) (*10*). Signals detected by all seven RDP4 algorithms were considered positive and validated by similarity analysis using SimPlot++ (version 1.3; Université du Québec à Montréal, Montréal, Canada) (*11*).

In total, 36 HMPV reference sequences representing different countries and years were downloaded from GenBank. Maximum-likelihood (ML) phylogenetic trees were constructed for the complete genome and the F and G genes using MEGA X (version 10.2; Temple University, Pennsylvania, United States) (*12*). The Kimura 2-parameter model was used for nucleotide substitution, with rate heterogeneity among sites modeled by a gamma distribution with invariant sites (G + I). Branch support was assessed using 1,000 bootstrap replicates. Recombinant sequences were excluded from the genome-wide ML tree.

Amino acid substitutions in the F and G proteins were analyzed. HMPV strains CAN97-83 (AY297749) and CAN98-75 (AY297748) were used as reference sequences for types A and B, respectively. F- and G-protein amino acid sequences were aligned using Clustal Omega (version 1.2.4) through the European Molecular Biology Laboratory-European Bioinformatics Institute (EMBL-EBI) web server (*13*). Selected mutation sites were mapped onto experimentally determined F-protein structures from the Research Collaboratory for Structural Bioinformatics Protein Data Bank (RCSB PDB) and visualized using ChimeraX (version 1.1.2; University of California, San Francisco, United States) (*14–15*). NetNGlyc-1.0 (version 1.0; https://services.healthtech.dtu.dk/services/NetNGlyc-1.0/) and NetOGlyc-4.0 (version 4.0; https://services.healthtech.dtu.dk/services/NetOGlyc-4.0/) were used to predict N-linked and O-linked glycosylation sites in the F and G proteins. Sites with scores >0.5 were considered glycosylated.

Data Analysis and Visualization

Differences in HMPV epidemiological patterns by age and season were assessed using chi-square tests. Peak HMPV positivity rates were compared using the Mann–Whitney U test in GraphPad Prism 9 (version 9.5.0; Dotmatics; Boston, MA, United States), with $\alpha = 0.05$. Figures were prepared using Adobe Illustrator 2023 (version 27.0; Adobe, San Jose, CA, United States), Python (version 3.9; Python Software Foundation, Wilmington, DE, United States), and Servier Medical Art (https://smart.servier.com).

RESULTS

Epidemic Pattern of HMPV in Children from 2012 to 2024 in Tianjin

In total, 8,325 throat swabs from pediatric outpatients with ILI during 2012–2024 were tested for HMPV by qRT-PCR (Figure 1A). HMPV was detected in 290 samples, and the overall positivity rate was 3.48% (290/8,325).

The highest annual positivity rate occurred in 2012, at 5.56% (21/378) (Figure 1B). The rate declined steadily during 2012–2017 and increased to 3.98% (26/653) in 2018. It declined again during the coronavirus disease 2019 (COVID-19) pandemic (2020–2022). The positivity rate increased by 2.05 percentage points from 2.47% (14/566) in 2022 to 4.52% (42/930) in 2023 and rose further to 4.73% (39/825) in 2024.

HMPV infection showed a significant seasonal pattern in Tianjin (χ^2=108.3, P<0.001) (Figure 1C). Positivity rates were highest in winter and spring, at 3.90% (124/3,179) and 6.94% (118/1,700), respectively. Significant spring peaks occurred in 2014 (16/127, 12.60%), 2018 (18/126, 14.29%), and 2023 (25/190, 13.16%) (U=0, P=0.007).

Participants were categorized into three age groups: <3 years, 3 to under 6 years, and ≥6 years. The corresponding positivity rates were 3.12% (104/3,337), 4.47% (134/2,995), and 2.61% (52/1,993), respectively, and differed significantly among groups (χ^2=14.61, P<0.001). Children aged 3–6 years accounted for the largest proportion of HMPV-positive cases (134/290, 46.2%) (Figure 1D).

HMPV-positive samples were subtyped by subtype-specific qRT-PCR, yielding 281 subtyped cases: 175 type A (175/281, 62.28%) and 106 type B (106/281, 37.72%). Type A predominated in 2012–2013, 2018–2019, and 2022–2024, whereas type B predominated in 2014, 2017, and 2020–2021. The proportions of types A and B were similar in 2015–2016 (Figure 1E). The dominant HMPV type in Tianjin thus shifted approximately every 1–3 years.

Genotyping and Recombination of HMPV from 2012 to 2024 in Tianjin

Using Nextclade version 3.21.0, the 79 HMPV genomes were classified into four subtypes: A2b (1/79, 1.27%), A2c (58/79, 73.42%), B1 (7/79, 8.86%), and B2 (13/79, 16.45%).

Among the 40 complete genome sequences, four recombination signals were identified, three between the A2c and B2 subtypes (Figure 2A–C). A fourth occurred between a 2012 B1 strain (HMPV/Tianjin/256/2012) and a 2023 A2c strain (HMPV/Tianjin/305/2023) (Figure 2D). The signals were located primarily within the L gene (7,076–13,093 bp) and were validated by similarity analysis using SimPlot++ (Supplementary Figure S2, available at https://weekly.chinacdc.cn/).

Phylogenetic Analysis and Genetic Variation of HMPV from 2012 to 2024 in Tianjin

Clustering in the genome-wide HMPV phylogenetic tree was consistent with the Nextclade subtype assignments (Figure 3A). An ML tree based on the conserved F gene included 1 A2b, 57 A2c, 7 B1, and 14 B2 sequences (Figure 3B). A2c predominated in 2018 (12/57, 21.05%), and detections increased again in 2023 (8/57, 14.04%) and 2024 (9/57, 15.79%). A2b was also detected in Tianjin in 2024. Neither B1 nor B2 showed clear temporal dominance.

G-gene phylogenetic clustering was consistent with F-gene classification (Figure 3C). However, in one strain (HMPV/Tianjin/31/2024), the G gene was classified as A2c and the F gene as B2 (Figure 3B). No recombination signal was confirmed in this sequence. In the genome-wide ML tree, it was assigned to A2c, consistent with the Nextclade result (Figure 3A). This discordance suggests substantial genetic variability in this strain.

In the G protein, substitutions to asparagine occurred at positions 122 and 145 in type A and at positions 101, 164, and 204 in type B, increasing predicted N-linked glycosylation sites (Supplementary Figure S3, available at https://weekly.chinacdc.cn/). Because the F protein mediates membrane fusion, substitutions in this protein may affect viral entry. The F protein contained 22 substitutions in type A and 27 in type B (Supplementary Table S4, available at https://weekly.chinacdc.cn/). Selected mutation sites were mapped onto F-protein structures (Figure 4A–B) (*16–17*). One O-linked glycosylation site at serine 444 (S444) was identified in all A2c strains, whereas 1–3 were identified in different type B strains at S85, S364, and threonine 521 (T521). Three N-linked glycosylation sites were identified at N57, N172, and N353 in both HMPV types.

Among 58 HMPV-A2c G-protein sequences, 22 (37.93%, 22/58) contained a 111-nt duplication

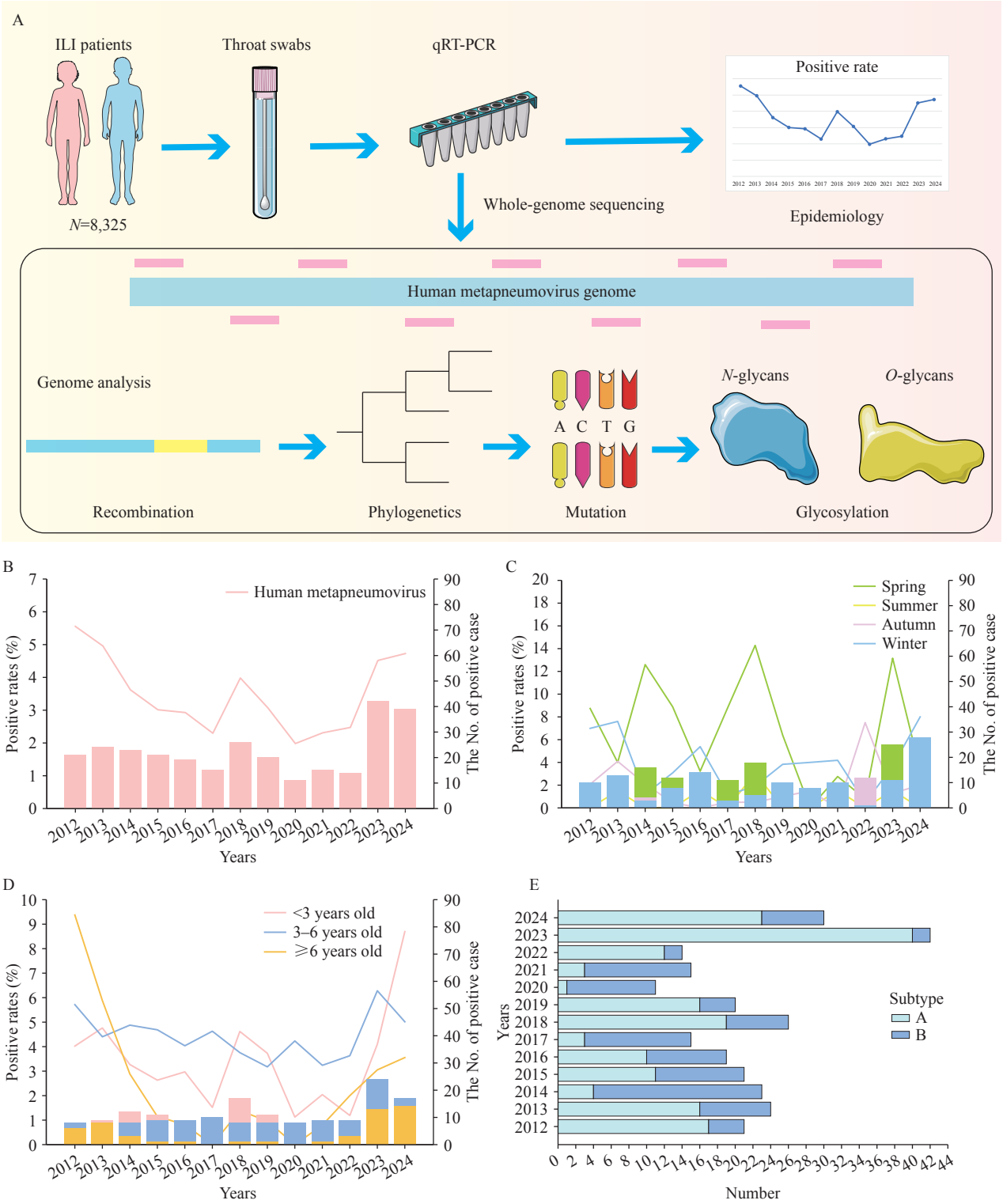

FIGURE 1. Epidemiological pattern of human metapneumovirus (HMPV) in Tianjin, 2012–2024. A. Schematic of the study design. B–D. Number of HMPV-positive samples (bars) and positivity rates (lines) by year (B), season (C), and age group (D) in Tianjin from 2012 to 2024. E. Proportions of HMPV types A and B in Tianjin from 2012 to 2024.

Note: (A) HMPV-positive samples are confirmed by qRT-PCR, and whole-genome sequencing is performed using primers designed in this study. (B)–(D), the x-axis indicates year. The left y-axis indicates the positivity rate, and the right y-axis indicates the number of positive samples. (E), the x-axis indicates the number of positive samples, and the y-axis indicates year.

Abbreviation: ILI=influenza-like illness; qRT-PCR=quantitative reverse-transcription polymerase chain reaction.

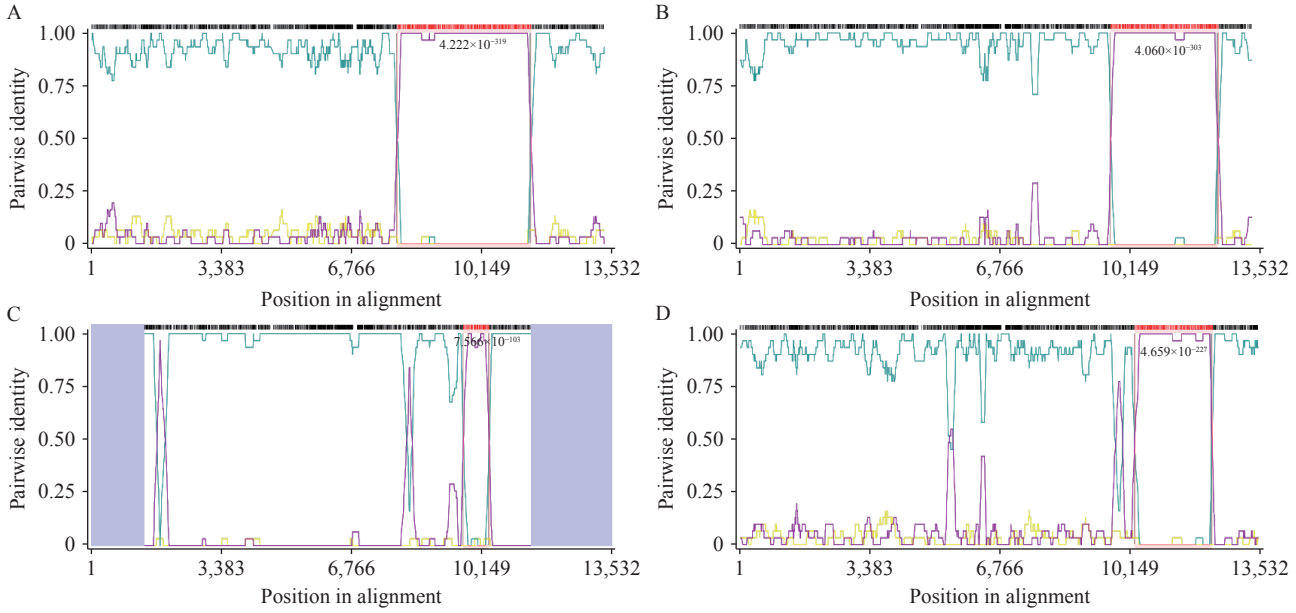

FIGURE 2. Recombination in HMPV genomes collected in Tianjin from 2012 to 2024. (A) Recombination signal between an A2c strain (HMPV/Tianjin/367/2023) and a B2 strain (HMPV/Tianjin/422/2024). (B) Recombination signal between an A2c strain (HMPV/Tianjin/367/2023) and a B2 strain (HMPV/Tianjin/106/2019). (C) Recombination signal between an A2c strain (HMPV/Tianjin/125/2024) and a B2 strain (OR883667-HMPV/Tianjin/44/2021). (D) Recombination signal between an A2c strain (HMPV/Tianjin/305/2023) and a B1 strain (HMPV/Tianjin/256/2012).
Note: Sequence maps of the four recombinant HMPV genomes generated using Recombination Detection Program version 4 (RDP4). The x-axis indicates the alignment position, and the y-axis indicates pairwise identity with the reference strains. Colored lines represent different parental strain pairs, and red regions indicate recombination signals. Cases detected by all seven algorithms are confirmed as recombination signals.
Abbreviation: HMPV=human metapneumovirus; RDP4=recombination detection program version 4.

spanning nucleotides 421–531; no 180-nt duplication was detected (Figure 4C). $A2c_{111nt\text{-}dup}$ strains emerged in 2017 and were detected during 2018–2024 except in 2020. The duplication increased G-protein length by 37 amino acids, and 4–11 O-linked glycosylation sites were predicted within the duplicated regions. One N-linked glycosylation site at N145 was identified in the duplicated regions of six sequences.

DISCUSSION

HMPV imposes a substantial annual healthcare burden (*8*). This study characterized the epidemiological and genetic features of HMPV infection in children in Tianjin during 2012–2024.

HMPV infection shows a distinct seasonal pattern in northern China, circulating from December through April and peaking between January and March (*18*). We observed a similar pattern in Tianjin, with the highest positivity rates in winter and spring. HMPV positivity was lower during 2020–2022 than in other study years, possibly because of nonpharmaceutical interventions (NPIs) during the COVID-19 pandemic (*19*).

Global estimates indicate that HMPV accounts for approximately 4%–10% of ARTIs in hospitalized children, imposing a substantial burden on pediatric healthcare systems (*20*). In this study, HMPV positivity was highest among children aged 3–6 years, overlapping with the finding in a recent review (*21*). This pattern may reflect fewer social contacts among children aged 0–3 years and greater immunity among those aged ≥6 years.

Phylogenetic analysis showed co-circulation of multiple HMPV subtypes, with one subtype usually predominating. The dominant type alternated between HMPV-A and HMPV-B every 1–3 years. A2c has predominated in recent years, consistent with observations elsewhere in China and worldwide (*18*,*22*).

Recombination may enable viruses to evade host immunity, expand their host range, or generate novel strains, but evidence for recombination in HMPV remains limited (*23*). We identified at least four recombination signals between HMPV types A and B, particularly after the COVID-19 pandemic; these were

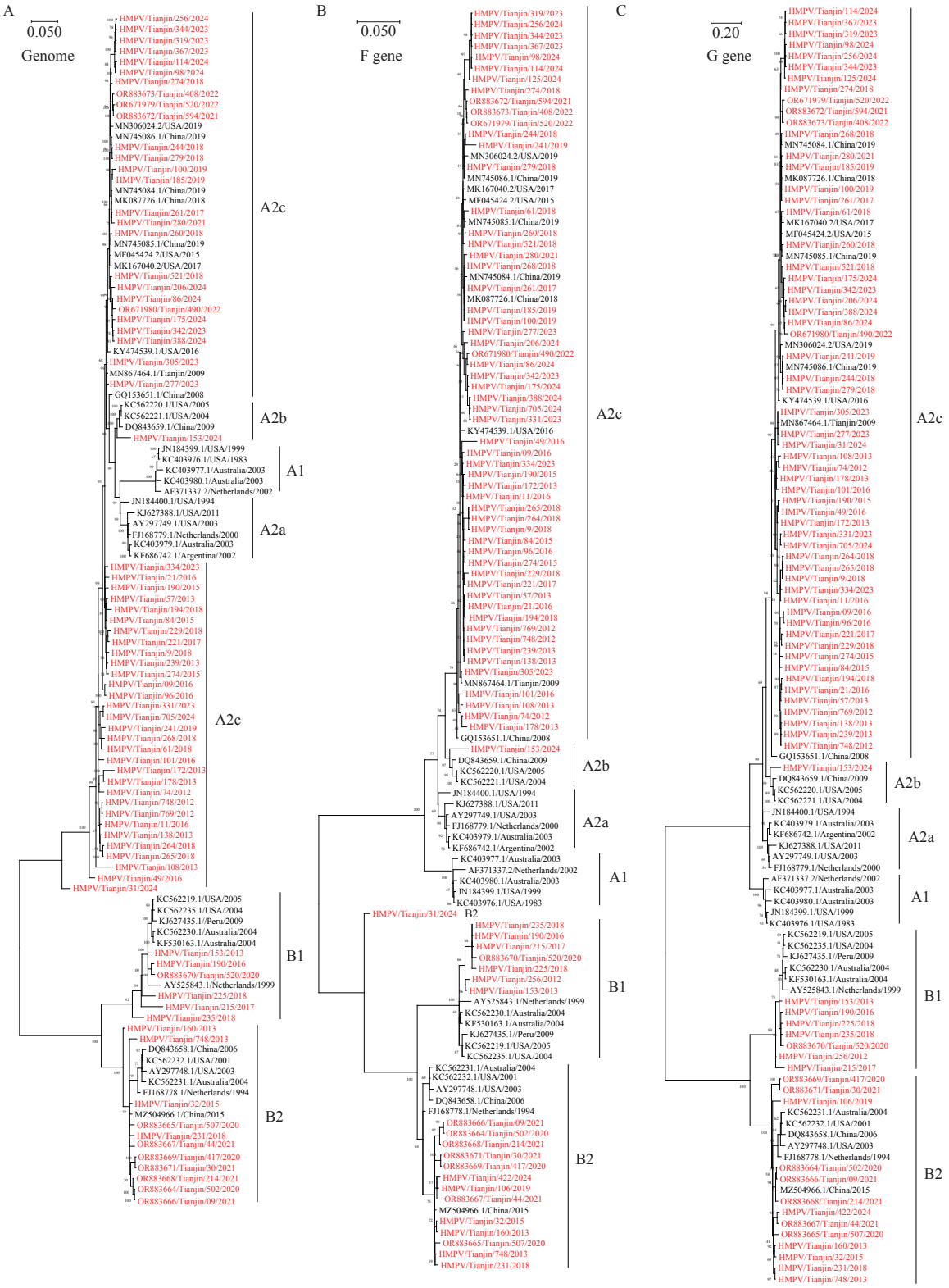

FIGURE 3. Phylogenetic trees of HMPV sequences collected in Tianjin from 2012 to 2024. (A) Maximum-likelihood (ML) tree based on the HMPV genome. (B) ML tree based on the F gene. (C) ML tree based on the G gene.

Note: All trees were constructed using MEGA X with 1,000 bootstrap replicates. Sequences generated in this study are shown in red, and reference sequences are shown in black. Scale bars appear in the upper-left corner, and bootstrap values indicate branch support.

Abbreviation: HMPV=human metapneumovirus; ML=maximum-likelihood.

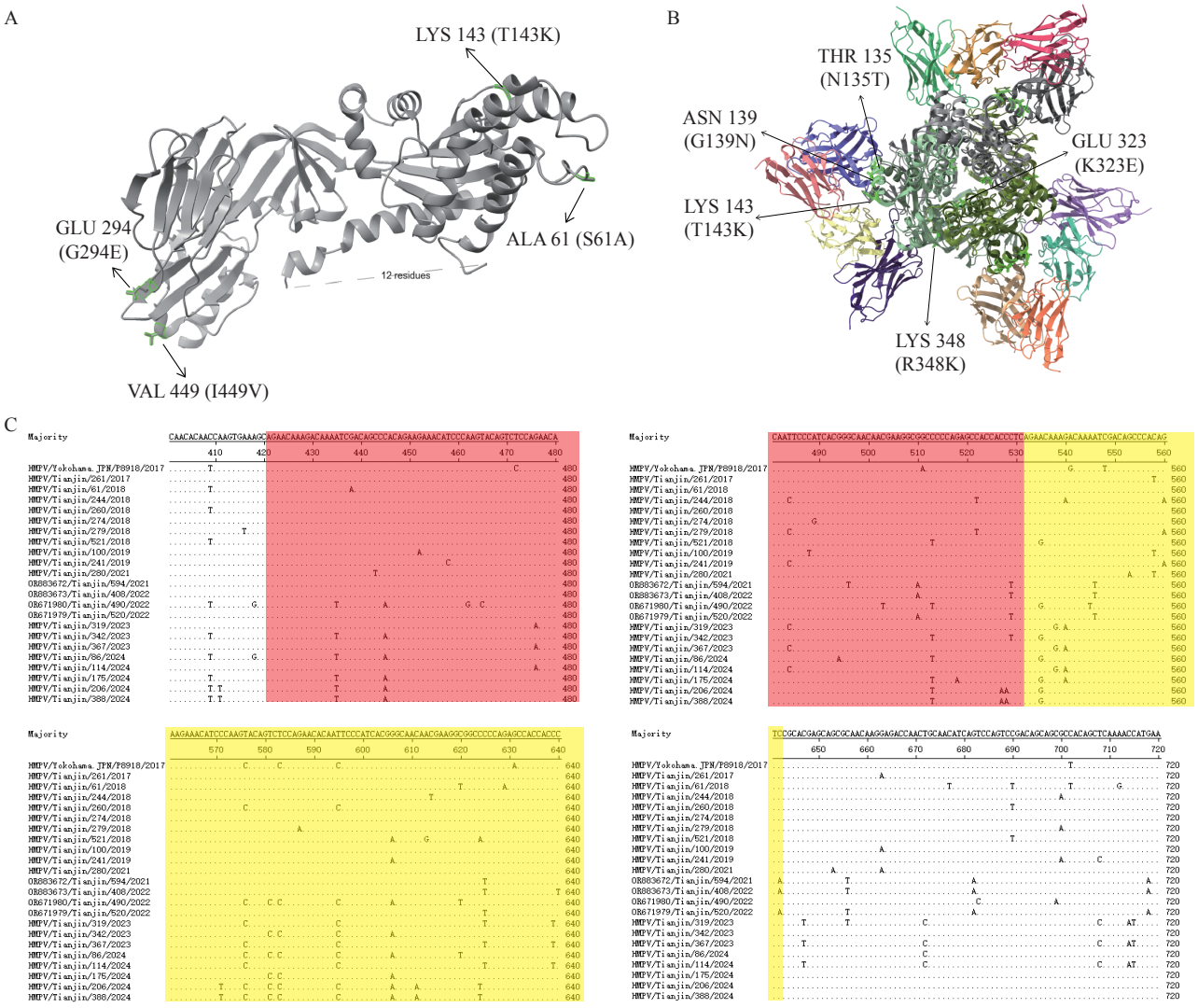

FIGURE 4. Genetic variation in the F and G proteins of HMPV strains. (A) Selected mutation sites in HMPV-A mapped onto an experimentally determined F-protein structure. (B) Selected mutation sites in HMPV-B mapped onto an experimentally determined F-protein structure. (C) The 111-nucleotide (nt) duplicated region in the HMPV G gene.
Note: (A) The structure is obtained from the Research Collaboratory for Structural Bioinformatics Protein Data Bank (RCSB PDB; PDB ID: 5WB0) and visualized using ChimeraX. (B) The structure is obtained from the RCSB PDB (PDB ID: 7TJQ) and visualized using ChimeraX. (C) Red and yellow indicate the first and second duplicated regions, respectively.
Abbreviation: HMPV=human metapneumovirus; nt=nucleotide; PDB=Protein Data Bank.

located primarily in the L gene. The L protein mediates the core catalytic activities of the viral polymerase complex (*24*). Chimeric HMPV-A1/HMPV-B1 polymerase complexes remained functional in vitro, with replication and transcription efficiencies comparable to those of wild-type complexes (*25*). Our findings underscore the potential transmission risk and the importance of routine molecular surveillance for novel recombinant strains.

The F protein is essential for membrane fusion during HMPV entry (*26*). Three mutations identified here, N135T, G139N, and T143K, lie within F-protein antigenic epitopes. These substitutions may affect neutralizing antibody binding to antigenic site V (*26*). N-linked glycosylation of viral envelope glycoproteins can modulate host antibody responses by shielding neutralization-sensitive epitopes (*27*). Glycosylation at N57 and N172 may mask the pre-fusion-specific antigenic site Ø near the trimer apex (*16*).

The G gene showed greater genetic variation than the F gene. A 111-nt duplication in the G gene defines the HMPV A2c111nt-dup variant, first detected in Japan in 2017 (*28*) and since widely reported in China

(*18*). In this study, the duplicated region occurred in 37.93% (22/58) of A2c sequences. The duplication increased predicted O-linked and N-linked glycosylation sites in the G protein. Glycans can protect viral polypeptide chains and suppress type I interferon responses, thereby promoting immune escape (*29*). Strains with duplicated regions have become predominant worldwide, but their effects on the clinical course of infection require further investigation (*22*).

These findings may inform HMPV prevention, control, and clinical management. Targeted public health interventions in high-risk populations, particularly school-based measures, should be implemented before the epidemic season. Screening in pediatric outpatient settings and early differential diagnosis by nucleic acid testing may reduce transmission. Routine pathogen monitoring and genomic surveillance by next-generation sequencing are important for assessing transmission risk.

This study has several limitations. Samples came from a single source. Larger, multicenter studies including all age groups and detailed clinical data are needed to further characterize HMPV epidemiological patterns. In addition, whole-genome sequencing coverage was insufficient for some strains because of low viral loads and poor RNA quality. More specific primers should therefore be optimized for such samples.

CONCLUSIONS

This study characterized the epidemiological pattern, seasonality, and age-related susceptibility of HMPV infection in children in Tianjin during 2012–2024. Genetic and molecular analyses identified recombination signals, amino acid substitutions, and glycosylation sites in the F and G proteins. These findings provide epidemiological and genomic evidence to inform HMPV prevention and control.

Acknowledgments: We thank the staff of Tianjin Children's Hospital and all study participants.

Conflicts of interest: No conflicts of interest.

Data availability statement: The data generated in this study are available in the supplementary materials. Sequence data have been deposited in the Science Data Bank (https://www.scidb.cn/en; DOI: 10.57760/sciencedb.28177). Additional data are available from the corresponding author upon reasonable request and with institutional permission.

Ethical statement: The Ethical Review Board of Tianjin Centers for Disease Control and Prevention approved this study (TJCDC-R-2022-017). Data were analyzed anonymously.

Funding: Supported by Tianjin Municipal Health Commission (TJWJ2022ZD010), Tianjin Key Medical Discipline (Specialty) Construction Project (TJYXZDXK-3-004D), and Tianjin Natural Science Foundation (25ZYCGSY01350).

doi: 10.46234/ccdcw2026.198

[#] Corresponding author: Xiaoyan Li, lixiaoyan6@tj.gov.cn.

[1] Institute of Microbiology, Tianjin Centers for Disease Control and Prevention, Tianjin, China; [2] Tianjin Key Laboratory of Pathogenic Microbiology of Infectious Disease, Tianjin Centers for Disease Control and Prevention, Tianjin, China; [3] Caofeidian District Center for Disease Control and Prevention, Tangshan City, Hebei Province, China; [4] Key Laboratory of Prevention and Control of Major Diseases in the Population, Ministry of Education, Tianjin Medical University, Tianjin, China.

[&] Joint first authors.

Copyright © 2026 by Chinese Center for Disease Control and Prevention & Chinese Academy of Preventive Medicine. All content is distributed under a Creative Commons Attribution Non Commercial License 4.0 (CC BY-NC).

Submitted: June 18, 2026
Accepted: September 29, 2026
Issued: October 02, 2026

REFERENCES

1. Jefferson T, Dooley L, Ferroni E, Al-Ansary LA, van Driel ML, Bawazeer GA, et al. Physical interventions to interrupt or reduce the spread of respiratory viruses. Cochrane Database Syst Rev 2023;1(1): CD006207. https://doi.org/10.1002/14651858.CD006207.pub6.
2. van den Hoogen BG, de Jong JC, Groen J, Kuiken T, de Groot R, Fouchier RAM, et al. A newly discovered human pneumovirus isolated from young children with respiratory tract disease. Nat Med 2001;7(6): 719 – 24. https://doi.org/10.1038/89098.
3. Rima B, Collins P, Easton A, Fouchier R, Kurath G, Lamb RA, et al. ICTV virus taxonomy profile: *Pneumoviridae*. J Gen Virol 2017;98(12): 2912 – 3. https://doi.org/10.1099/jgv.0.000959.
4. Xie ZB, Xu J, Ren YH, Cui AL, Wang HL, Song JH, et al. Emerging human metapneumovirus gene duplication variants in patients with severe acute respiratory infection, China, 2017-2019. Emerg Infect Dis 2021;27(1):275 – 7. https://doi.org/10.3201/eid2701.201043.
5. Feng Y, He T, Zhang B, Yuan HB, Zhou YF. Epidemiology and diagnosis technologies of human metapneumovirus in China: a mini review. Virol J 2024;21(1):59. https://doi.org/10.1186/s12985-024-02327-9.
6. Wang X, Li Y, Deloria-Knoll M, Madhi SA, Cohen C, Ali A, et al. Global burden of acute lower respiratory infection associated with human metapneumovirus in children under 5 years in 2018: a systematic review and modelling study. Lancet Glob Health 2021;9(1): e33 – 43. https://doi.org/10.1016/s2214-109x(20)30393-4.
7. Lüsebrink J, Wiese C, Thiel A, Tillmann RL, Ditt V, Muller A, et al. High seroprevalence of neutralizing capacity against human metapneumovirus in all age groups studied in Bonn, Germany. Clin Vaccine Immunol 2010;17(3):481 – 4. https://doi.org/10.1128/cvi.00398-09.
8. Ma SY, Zhu F, Xu YZ, Wen HC, Rao MJ, Zhang PP, et al. Development of a novel multi-epitope mRNA vaccine candidate to

combat HMPV virus. Hum Vaccin Immunother 2024;20(1):2293300. https://doi.org/10.1080/21645515.2023.2293300.
9. Aksamentov I, Roemer C, Hodcroft EB, Neher RA. Nextclade: clade assignment, mutation calling and quality control for viral genomes. J Open Source Softw 2021;6(67):3773. https://doi.org/10.21105/joss.03773.
10. Martin DP, Murrell B, Golden M, Khoosal A, Muhire B. RDP4: detection and analysis of recombination patterns in virus genomes. Virus Evol 2015;1(1):vev003. https://doi.org/10.1093/ve/vev003.
11. Samson S, Lord É, Makarenkov V. SimPlot++: a Python application for representing sequence similarity and detecting recombination. Bioinformatics 2022;38(11):3118 – 20. https://doi.org/10.1093/bioinformatics/btac287.
12. Kumar S, Stecher G, Li M, Knyaz C, Tamura K. MEGA X: molecular evolutionary genetics analysis across computing platforms. Mol Biol Evol 2018;35(6):1547 – 9. https://doi.org/10.1093/molbev/msy096.
13. Madeira F, Madhusoodanan N, Lee J, Eusebi A, Niewielska A, Tivey ARN, et al. The EMBL-EBI Job Dispatcher sequence analysis tools framework in 2024. Nucleic Acids Res 2024;52(W1):W521 – 5. https://doi.org/10.1093/nar/gkae241.
14. Berman HM, Westbrook J, Feng ZK, Gilliland G, Bhat TN, Weissig H, et al. The protein data bank. Nucleic Acids Res 2000;28(1):235 – 42. https://doi.org/10.1093/nar/28.1.235.
15. Meng EC, Goddard TD, Pettersen EF, Couch GS, Pearson ZJ, Morris JH, et al. UCSF ChimeraX: tools for structure building and analysis. Protein Sci 2023;32(11):e4792. https://doi.org/10.1002/pro.4792.
16. Battles MB, Más V, Olmedillas E, Cano O, Vázquez M, Rodríguez L, et al. Structure and immunogenicity of pre-fusion-stabilized human metapneumovirus F glycoprotein. Nat Commun 2017;8(1):1528. https://doi.org/10.1038/s41467-017-01708-9.
17. Rush SA, Brar G, Hsieh CL, Chautard E, Rainho-Tomko JN, Slade CD, et al. Characterization of prefusion-F-specific antibodies elicited by natural infection with human metapneumovirus. Cell Rep 2022;40(12):111399. https://doi.org/10.1016/j.celrep.2022.111399.
18. Li AH, Gong C, Wang L, Han YL, Kang L, Hu G, et al. Epidemiological and phylogenetic characteristics of human metapneumovirus in Beijing, China, 2014-2024. Signal Transduct Target Ther 2025;10(1):300. https://doi.org/10.1038/s41392-025-02377-7.
19. Huang QS, Wood T, Jelley L, Jennings T, Jefferies S, Daniells K, et al. Impact of the COVID-19 nonpharmaceutical interventions on influenza and other respiratory viral infections in New Zealand. Nat Commun 2021;12(1):1001. https://doi.org/10.1038/s41467-021-21157-9.
20. Brochado-Kith O, Gil-Prieto R, Gil-de-Miguel A. Epidemiological burden and hospitalization trends of human metapneumovirus in Spain (2016-2023): a retrospective study. Infect Dis Ther 2026;15(4):1115 – 35. https://doi.org/10.1007/s40121-026-01317-4.
21. Divarathna MVM, Rafeek RAM, Noordeen F. A review on epidemiology and impact of human metapneumovirus infections in children using TIAB search strategy on PubMed and PubMed Central articles. Rev Med Virol 2020;30(1):e2090. https://doi.org/10.1002/rmv.2090.
22. Siafakas N, Papadopoulou K, Psina A, Tsiodras S, Pournaras S. Emergence and molecular epidemiology of human metapneumovirus in Greece in the post-COVID era. Int J Mol Sci 2026;27(6):2821. https://doi.org/10.3390/ijms27062821.
23. Kim JI, Park S, Lee I, Park KS, Kwak EJ, Moon KM, et al. Genome-wide analysis of human metapneumovirus evolution. PLoS One 2016;11(4):e0152962. https://doi.org/10.1371/journal.pone.0152962.
24. Pan JH, Qian XL, Lattmann S, El Sahili A, Yeo TH, Jia H, et al. Structure of the human metapneumovirus polymerase phosphoprotein complex. Nature 2020;577(7789):275 – 9. https://doi.org/10.1038/s41586-019-1759-1.
25. de Graaf M, Herfst S, Schrauwen EJA, Choi Y, van den Hoogen BG, Osterhaus ADME, et al. Specificity and functional interaction of the polymerase complex proteins of human and avian metapneumoviruses. J Gen Virol 2008;89(Pt 4):975-83. http://dx.doi.org/10.1099/vir.0.83537-0.
26. Xiao X, Fridman A, Zhang L, Pristatsky P, Durr E, Minnier M, et al. Profiling of hMPV F-specific antibodies isolated from human memory B cells. Nat Commun 2022;13(1):2546. https://doi.org/10.1038/s41467-022-30205-x.
27. Gardner TJ, Tortorella D. Virion glycoprotein-mediated immune evasion by human cytomegalovirus: a sticky virus makes a slick getaway. Microbiol Mol Biol Rev 2016;80(3):663 – 77. https://doi.org/10.1128/mmbr.00018-16.
28. Saikusa M, Nao N, Kawakami C, Usuku S, Sasao T, Toyozawa T, et al. A novel 111-nucleotide duplication in the G gene of human metapneumovirus. Microbiol Immunol 2017;61(11):507 – 12. https://doi.org/10.1111/1348-0421.12543.
29. Bitko V, Barik S. Role of metapneumoviral glycoproteins in the evasion of the host cell innate immune response. Infect Genet Evol 2021;96:105096. https://doi.org/10.1016/j.meegid.2021.105096.

SUPPLEMENTARY MATERIALS

SUPPLEMENTARY TABLE S1. Primers used for human metapneumovirus (HMPV) whole-genome amplification.

Primer	Sequence (5′→3′)	Positions (nt)	Amplicon length (bp)
HMPV-1-F	GGGACAARTRAAAATGTCTCTTCA	41–64	
HMPV-1-R	TCTTTTRRTTCTTCYTCTTCTTCDGATT	2,070–2,097	2,057
HMPV-2-F	AGCAGCHGARATGATGGAAGARG	1,948–1,970	
HMPV-2-R	CTTCCTGTGCTRACTTTRCAYG	4,146–4,165	2,218
HMPV-3-F	ACAGCWGCAGGRATYAATGT	4,074–4,093	
HMPV-3-R	CATRTCTATYGCYCGAATGTTCTC	6,248–6,271	2,198
HMPV-4-F	GGGACAAGTRGYYATGGARGTR	6,220–6,241	
HMPV-4-R	TRGTRCTRAAYTGAGCATGYTCAG	8,095–8,118	1,899
HMPV-5-F	AACTGYTAACATGGAARGATGTGATG	7,858–7,883	
HMPV-5-R	TTCYTGACAYARACTYCCTATTGAY	9,764–9,788	1,931
HMPV-6-F	ACATGCACCACCAGAAAC	9,178–9,195	
HMPV-6-R	AGGTGTTATGTTKTCWGC	10,208–10,225	1,048
HMPV-7-F	GTGAYATMAATAGAACAGC	10,128–10,146	
HMPV-7-R	GGAATTAGYATAATGAGTG	11,231–11,248	1,121
HMPV-8-F	GGATATTCACATGCTGTTC	11,081–11,099	
HMPV-8-R	GGAATTAGYATAATGAGTG	12,246–12,264	1,184
HMPV-9-F	CTAACAAGRAATTACATG	12,071–12,088	
HMPV-9-R	ACGGCAAAAAAACCGTAT	13,318–13,335	1,265

Note: A total of 192 nucleic acid samples with cycle threshold (Ct) values ≤35 underwent whole-genome amplification and sequencing. Seventy-nine sequences had coverage ≥90%, including 40 complete genomes ranging from 13,045 to 13,390 nt. The remaining 39 sequences contained a deletion of approximately 1,000 bp at the seventh primer-binding site within the L-gene fragment.
Abbreviation: HMPV=human metapneumovirus; nt=nucleotide.

SUPPLEMENTARY TABLE S2. Reverse-transcription polymerase chain reaction system for HMPV complementary DNA synthesis.

Reaction system		Reaction program		
Reagent	Volume (μL)	Temperature (°C)	Time (min)	Cycles
SuperScript™ IV VILO™ (SSIV VILO) Master Mix	6	25	2	1
Nucleic acid	6	55	10	1
ddH_2O	18	95	1	1

Abbreviation: HMPV=human metapneumovirus; DNA=deoxyribonucleic acid; ddH_2O=double-distilled water.

SUPPLEMENTARY TABLE S3. Polymerase chain reaction (PCR) system for HMPV genome amplification.

Reaction system		Reaction program		
Reagent	Volume (μL)	Temperature (°C)	Time	Cycles
Platinum™ SuperFi™ PCR Master Mix	12.5	98	30 s	1
Forward Primer (10 μmol/L)	1.25	94	10 s	
Reverse Primer (10 μmol/L)	1.25	$T_m - 5$	20 s	44
ddH_2O	7	72	1 kb/min	
cDNA	3	72	5 min	1
Total	25	4	Hold	

Abbreviation: HMPV=human metapneumovirus; PCR=polymerase chain reaction; ddH_2O=double-distilled water; cDNA=complementary DNA.

SUPPLEMENTARY TABLE S4. Amino acid substitutions in the HMPV F protein.

Substitution	Number of type A sequences	Substitution	Number of type B sequences
V6M	1	M6V	1
F9L	8	M6T	1
F9I	1	L36H	4
V47I	1	E96G	1
S61A	58	N135T	1
S101P	1	G139N	1
T143K	58	T143Q	7
N145S	1	T143K	1
K166E	1	K179R	9
K171R	2	T223N	12
T223N	1	D280N	12
F256L	1	D296N	7
G294E	58	K323E	19
K348R	1	R348K	1
V424I	1	I392T	11
I449V	57	R396Q	11
K450R	1	P404N	1
S503F	2	S444N	12
I510V	1	K450R	19
T517A	1	D475E	5
K518R	32	N482S	1
A523E	1	N482D	1
		I498V	7
		T517A	2
		T521A	11
		T531A	1
		G533S	1

Abbreviation: HMPV=human metapneumovirus.

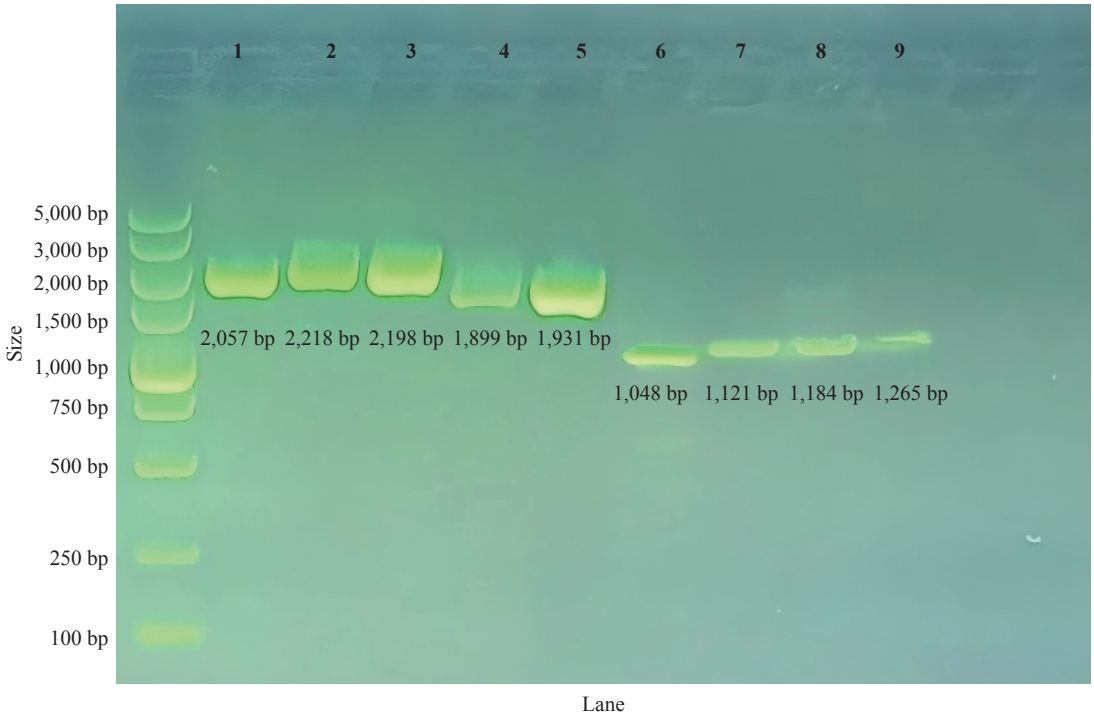

SUPPLEMENTARY FIGURE S1. Agarose gel electrophoresis of HMPV genomic amplification products generated with the newly designed primers.
Note: Numbers above the lanes indicate the corresponding newly designed primer pairs.
Abbreviation: HMPV=human metapneumovirus.

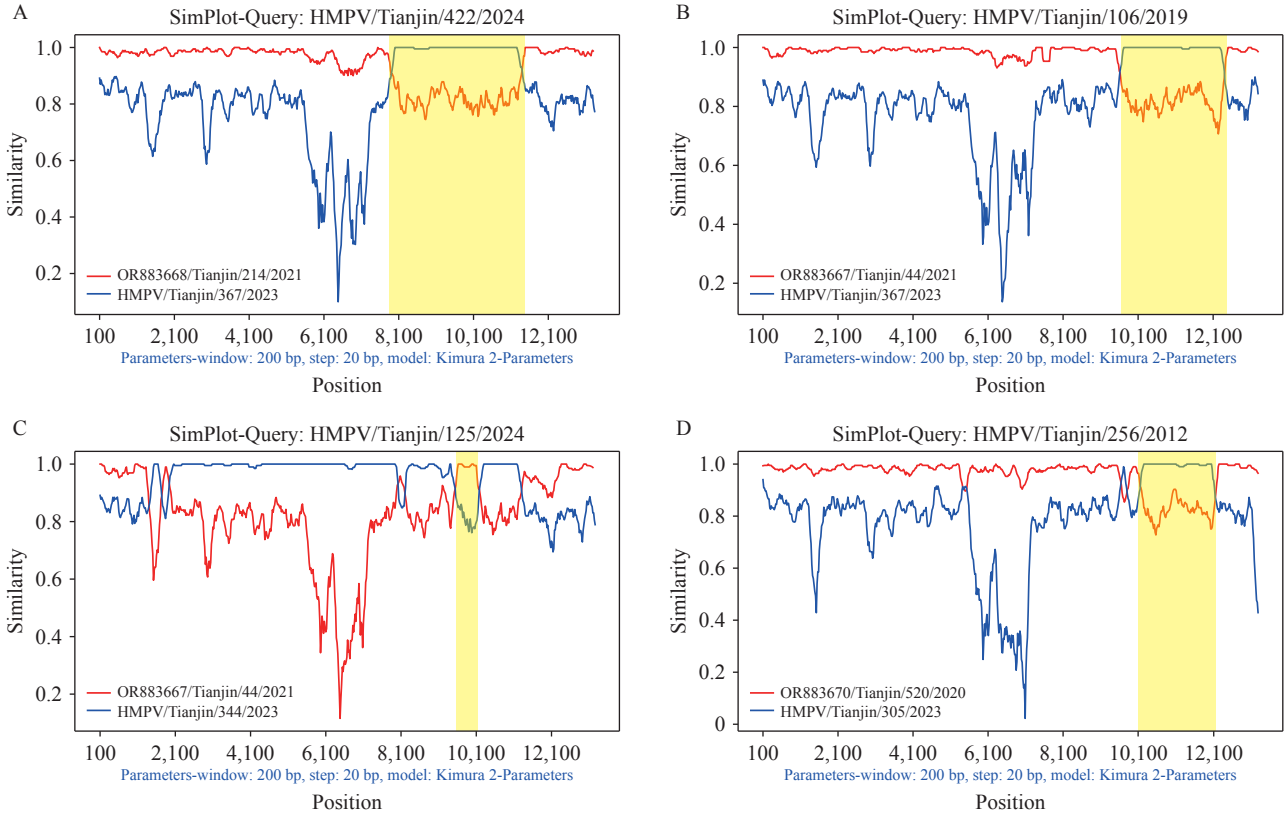

SUPPLEMENTARY FIGURE S2. SimPlot validation of recombination signals. (A) Recombination signal between an A2c strain (HMPV/Tianjin/367/2023) and a B2 strain (HMPV/Tianjin/422/2024). (B) Recombination signal between an A2c strain (HMPV/Tianjin/367/2023) and a B2 strain (HMPV/Tianjin/106/2019). (C) Recombination signal between an A2c strain (HMPV/Tianjin/125/2024) and a B2 strain (OR883667-HMPV/Tianjin/44/2021). (D) Recombination signal between an A2c strain (HMPV/Tianjin/305/2023) and a B1 strain (HMPV/Tianjin/256/2012).
Note: Sliding-window similarity analysis uses a window size of 200 bp, a step size of 20 bp, and the Kimura 2-parameter distance model. Gaps are removed when present in >33% of sequences.

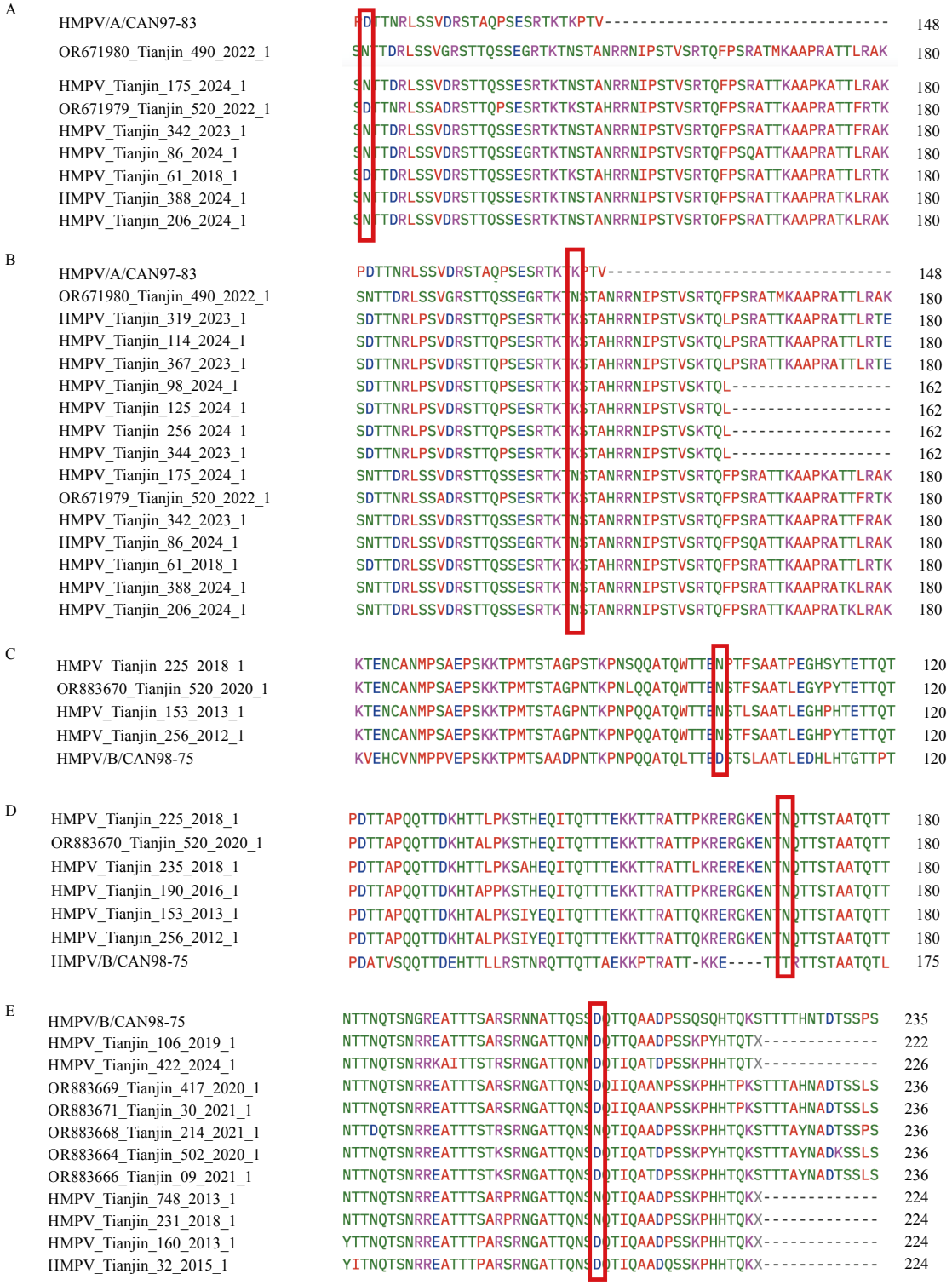

SUPPLEMENTARY FIGURE S3. Asparagine substitutions in the G protein increase N-linked glycosylation sites in HMPV. (A) D122N substitution in HMPV type A, resulting in an additional predicted N-linked glycosylation site. (B) K145N substitution in HMPV type A, resulting in an additional predicted N-linked glycosylation site. (C) D101N substitution in HMPV type B, resulting in an additional predicted N-linked glycosylation site. (D) T164N substitution in HMPV type B, resulting in an additional predicted N-linked glycosylation site. (E) D204N substitution in HMPV type B, resulting in an additional predicted N-linked glycosylation site.

Note: Asparagine substitutions in the G protein are outlined in red.

Methods and Applications

Safety of PCV13 with Different Carrier Proteins (CRM197, TT, and TT/DT) — Jiangsu Province, China, 2022–2024

Xun Li[1]; Borong Xu[1]; Zhiguo Wang[1]; Hongxiong Guo[1]; Yuanyuan Zhu[1]; Ran Hu[1]; Jing Yu[1,#]

ABSTRACT

Introduction: This study aimed to evaluate the safety of three kinds of 13-valent pneumococcal conjugate vaccines (PCV13) with different carrier proteins — cross-reactive material 197 (CRM197), tetanus toxoid (TT), and a novel tetanus toxoid/diphtheria toxoid (TT/DT) dual-carrier — by monitoring adverse events following immunization (AEFI) in Jiangsu Province, China.

Methods: The Chinese National Adverse Events Following Immunization Information System and Jiangsu Province Vaccination Integrated Service Management Information System were used. Reporting rates (RR) per 100,000 doses were calculated and stratified. Chi-square tests with Bonferroni correction and disproportionality analyses were performed.

Results: A total of 1,734,810 PCV13 doses were administered, with 5,195 AEFI reports (RR=299.46 per 100,000 doses). RR was highest for TT/DT-carrier (399.84 per 100,000 doses) versus CRM197-carrier (286.69 per 100,000 doses) and TT-carrier (286.01 per 100,000 doses). Common adverse reactions accounted for 98.23% (5,103/5,195) of all AEFIs, with fever, local redness, and induration being the most common. Disproportionality analysis revealed positive signals for general reactions.

Conclusion: All three PCV13 carrier protein types demonstrated acceptable safety profiles in Jiangsu Province from 2022 to 2024. Despite a higher RR for TT/DT-carrier PCV13 than for the other two PCV13 carrier protein types, most AEFIs were mild and common reactions.

Streptococcus pneumoniae is the most common pathogen responsible for community-acquired pneumonia, bacterial meningitis, bacteremia, and acute otitis media, posing a serious threat to the health of infants and young children (*1*).

The pneumococcal conjugate vaccine (PCV) has been recommended by the World Health Organization (WHO) for inclusion in routine childhood immunization programs worldwide, demonstrating favorable efficacy and safety in preventing invasive pneumococcal disease and pneumonia (*1*). The currently available 13-valent PCV (PCV13) can be classified by the carrier protein type: single-carrier PCV13 using cross-reactive material 197 (CRM197, a nontoxic mutant of diphtheria toxin) or tetanus toxoid (TT), and the recently developed dual-carrier PCV13 using tetanus toxoid/diphtheria toxoid (TT/DT). The introduction of PCV13 in China has followed a phased pathway: imported PCV13 in 2016, domestic TT-carrier PCV13 in early 2020, and TT/DT dual-carrier PCV13 in 2021 (*2*). However, PCV13 has not yet been integrated into China's National Immunization Program; as a self-paid vaccine, its coverage has remained low and unevenly distributed across regions (*3*).

Post-marketing safety surveillance, as recommended by the WHO, is essential for evaluating vaccine safety in real-world settings. Since 2019, multiple PCV13s with different carrier protein types have been introduced in Jiangsu Province, China. Previous studies have evaluated the safety of CRM197- and TT-carrier PCV13s during 2019–2022, confirming that both have favorable safety profiles (*4*). However, a parallel comparison of the three carrier protein types (CRM197, TT, and TT/DT) of PCV13, particularly the real-world safety data for the TT/DT dual-carrier PCV13 after its market introduction, has not yet been reported.

This study analyzed adverse events following immunization (AEFI) reports for three PCV13 types in Jiangsu from 2022 to 2024 using the Jiangsu Province Vaccination Integrated Service Management Information System (JSEIRS) and the Chinese National Adverse Events Following Immunization Information System (CNAEFIS) to characterize the AEFI incidence and distribution for post-marketing

 Copyright © 2026 by Chinese Center for Disease Control and Prevention

safety evaluation.

METHODS

Data Source

Data were obtained from two information systems. Vaccination data were extracted from the JSEIRS, and AEFI data were sourced from the CNAEFIS (Supplementary Materials, available at https://weekly.chinacdc.cn/).

All PCV13 vaccination records and associated AEFI reports in Jiangsu Province from January 1, 2022, to December 31, 2024, were extracted. Cases with missing essential variables (e.g., age, vaccine type, and outcome) or duplicate records were excluded.

Vaccination Schedule for PCV13

The immunization schedule for all three PCV13s comprises three primary doses, followed by one reinforced dose (*5*). Immunization can be initiated as early as six weeks of age, with an interval of at least one month between doses. The reinforced dose is administered at 12–15 months of age. The TT-carrier PCV13 has a wider age indication, being applicable to children aged 6 weeks to 5 years.

AEFI Categorization

According to *the National Guideline for the Surveillance of Adverse Events Following Immunization* (*6*), AEFIs are classified into five types: adverse reactions (including common and rare adverse reactions), vaccine quality defect-related events, immunization error-related adverse events, immunization anxiety-related reactions, and coincidental events. AEFI symptoms and diagnoses were coded according to the International Classification of Diseases, Tenth Revision (ICD-10).

Data Analysis

Data analysis was performed using R (version 4.5.2; R Foundation, Vienna, Austria). The AEFI reporting rate (RR) per 100,000 doses of PCV13 administered was calculated. Bonferroni correction was applied to account for multiple comparisons, with a two-tailed significance level of $\alpha = 0.05$.

The Proportional Reporting Ratio (PRR), Reporting Odds Ratio (ROR), Medicines and Healthcare Products Regulatory Agency (MHRA) comprehensive standard method, and Bayesian Confidence Propagation Neural Network (BCPNN) method were used for disproportionality analysis (DPA) of AEFI reports. DPA was computed using the *PhViD* package (version 1.0.8) in R (Supplementary Materials, available at https://weekly.chinacdc.cn/).

RESULTS

From January 2022 to December 2024, 1,734,810 PCV13 doses were administered in Jiangsu Province: 898,533 CRM197-carrier (51.79%, 898,533/1,734,810), 636,698 TT-carrier (36.70%, 636,698/1,734,810), and 199,579 TT/DT-carrier (11.50%, 199,579/1,734,810). A total of 5,195 AEFI reports were recorded, yielding an overall RR of 299.46 per 100,000 doses (Table 1).

The AEFI RR varied significantly by age group, sex, region, vaccine type, and dose number (all $P<0.001$), except between children aged 1–2 and 2–3 years, CRM197-carrier and TT-carrier vaccines, and first *vs*. second, first *vs*. fourth, and second *vs*. fourth doses. (Table 2). Common adverse reaction RR was generally higher in children >3 years, males, and Southern Jiangsu, though common adverse reactions were highest with TT/DT-carrier vaccines and after the second dose, while rare adverse reactions and coincidental events were highest with CRM197-carrier vaccines, and after the first and fourth doses, respectively (Table 3).

For CRM197-carrier PCV13, 2,519 cases (49.36%) had common adverse reactions (fever, local redness, induration); fever peaked at 37.6–38.5 °C, with redness and induration most common at 2.6–5.0 cm (Figure 1A, 1B). TT-carrier and TT/DT-carrier PCV13 saw 1,792 (35.12%) and 792 (15.52%) common reactions, respectively; fever was most frequent at ≥38.6 °C, with redness and induration most common at 2.6–5.0 cm (Figure 1C–1F). The top five non-common AEFI symptoms were sweating, nausea, fatigue, abdominal pain, and diarrhea (Supplementary Table S1, available at https://weekly.chinacdc.cn/).

The DPA of the final clinical diagnoses for 5,195 AEFI cases was performed using PRR, ROR, MHRA, and BCPNN. The diagnosis of general reactions (fever/redness/induration) showed positive signals across all four methods (PRR-1.96SE=6.61; ROR-1.96SE=165.38; MHRA: AEFI cases=5,042, PRR=6.79, χ^2=24,912.69; BCPNN: IC-2SD=2.72) (SE=standard error; IC-2SD=lower limit of IC 95% confidence intervals)(Table 4).

Furthermore, the DPA of the AEFI reports

TABLE 1. PCV13 vaccination and AEFI reports in Jiangsu Province from 2022 to 2024.

Group	Total			CRM197-carrier protein			TT-carrier protein			TT/DT-carrier protein		
	Vaccine doses (%)	AEFI cases	RR (per 100,000 doses)	Vaccine doses (%)	AEFI cases	RR (per 100,000 doses)	Vaccine doses (%)	AEFI cases	RR (per 100,000 doses)	Vaccine doses (%)	AEFI cases	RR (per 100,000 doses)
Total	1,734,810 (100)	5,195	299.46	898,533 (51.79)	2,576	286.69	636,698 (36.70)	1,821	286.01	199,579 (11.50)	798	399.84
Year												
2022	603,739 (34.80)	1,253	207.54	308,304 (34.31)	605	196.23	270,107 (42.42)	578	213.99	25,328 (12.69)	70	276.37
2023	623,271 (35.93)	1,821	292.17	310,054 (34.51)	853	275.11	229,723 (36.08)	623	271.20	83,494 (41.84)	345	413.20
2024	507,800 (29.27)	2,121	417.68	280,175 (31.18)	1,118	399.04	136,868 (21.50)	620	452.99	90,757 (45.47)	383	422.01
Dose												
1st dose	493,129 (28.43)	1,532	310.67	237,926 (26.48)	793	333.30	178,917 (28.10)	461	257.66	76,286 (38.22)	278	364.42
2nd dose	460,590 (26.55)	1,476	320.46	229,448 (25.54)	606	264.11	173,940 (27.32)	624	358.74	57,202 (28.66)	246	430.05
3rd dose	413,984 (23.86)	1,060	256.05	219,587 (24.44)	525	239.09	153,304 (24.08)	380	247.87	41,093 (20.59)	155	377.19
4th dose	367,088 (21.16)	1,127	307.01	211,564 (23.55)	652	308.18	130,528 (20.50)	356	272.74	24,996 (12.52)	119	476.08
Reaction type												
Common adverse reactions	–	5,103	294.15	–	2,519	280.35	–	1,792	281.45	–	792	396.84
Rare adverse reactions	–	50	2.88	–	30	3.34	–	16	2.51	–	4	2.00
Coincidental event	–	42	2.42	–	27	3.00	–	13	2.04	–	2	1.00
Severity												
Serious	–	11	0.63	–	8	0.89	–	3	0.47	–	0	0.00
Non-serious	–	5,184	298.82	–	2,568	285.80	–	1,818	285.54	–	798	399.84
Time interval												
≤30 min	–	53	3.06	–	19	2.11	–	20	3.14	–	14	7.01
30 min<Time≤1 day	–	3,571	205.84	–	1,825	203.11	–	1,234	193.81	–	512	256.54
1 day<Time≤3 days	–	1,287	74.19	–	584	64.99	–	465	73.03	–	238	119.25
>3 days	–	284	16.37	–	148	16.47	–	102	16.02	–	34	17.04

Note: "–": Dash indicates data not available.
Abbreviation: PCV13=13-valent pneumococcal conjugate vaccine; AEFI=adverse events following immunization; CRM197=cross-reactive material 197; TT=tetanus toxoid; TT/DT=tetanus toxoid/diphtheria toxoid; RR=reporting rate (per 100,000 doses).

associated with each of the three PCV13 types is presented in Supplementary Tables S2–S4 (available at https://weekly.chinacdc.cn/). For CRM197-carrier PCV13, positive signals for allergic rash were detected using the PRR and ROR methods (PRR-1.96SE=1.11; ROR-1.96SE=1.11). For TT-carrier PCV13, positive signals for general reactions (fever/redness/induration) were detected using the PRR and ROR methods (PRR-1.96SE=1.00; ROR-1.96SE=1.03). For TT/DT-carrier PCV13, no positive signals were detected using any of the four methods.

DISCUSSION

Based on large-scale passive surveillance data from Jiangsu Province, this study investigated the post-marketing safety of three PCV13s with different carrier protein types between 2022 and 2024. The overall reported AEFI RR for PCV13 was 299.46 per 100,000 doses, which was slightly higher than the PCV13 surveillance results from Jiangsu Province in 2019–2022 (186.80 per 100,000 doses) (*4*) and Zhejiang Province in 2022 (175.8 per 100,000 doses) (*7*). This discrepancy may be attributed to improved AEFI surveillance sensitivity, the new introduction of TT/DT-carrier PCV13, and increased public awareness of vaccine safety.

This study is the first post-marketing safety evaluation of the TT/DT dual-carrier PCV13 in Jiangsu Province, China. The results showed that the AEFI reporting rate for the TT/DT-carrier PCV13

TABLE 2. Characteristics of AEFI after PCV13 in Jiangsu Province from 2022 to 2024.

Group	Total				2022		2023		2024	
	AEFI cases (%)	RR (per 100,000 doses)	χ^2	*P*	AEFI cases (%)	RR (per 100,000 doses)	AEFI cases (%)	RR (per 100,000 doses)	AEFI cases (%)	RR (per 100,000 doses)
Age										
<1 year	3,508 (67.53)	284.53	241.03	<0.001[&]	821 (65.62)	187.15	1,261 (69.25)	288.90	1,426 (67.23)	398.59
1 year≤Age<2 years	1,491 (28.70)	320.79*			381 (30.41)	252.12	472 (25.92)	275.31	638 (30.08)	448.60
2 years≤Age<3 years	48 (0.92)	259.40*			12 (0.96)	161.99	21 (1.15)	293.62	15 (0.71)	373.51
≥3 years	148 (2.85)	957.37			39 (3.11)	748.42	67 (3.68)	942.07	42 (1.98)	1339.29
Sex										
Male	2,882 (55.48)	321.07	28.97	<0.001[&]	705 (56.26)	224.74	1,021 (56.07)	317.33	1,156 (54.50)	440.93
Female	2,313 (44.52)	276.28			548 (43.74)	188.93	800 (43.93)	265.32	965 (45.50)	392.87
Region										
Southern Jiangsu	3,339 (64.27)	307.66[†]	9.82	<0.001[&]	820 (65.44)	220.21	1,213 (66.61)	311.29	1,306 (61.57)	404.01
Central Jiangsu	745 (14.34)	271.38[§]			200 (15.96)	203.30	228 (12.52)	238.34	317 (14.95)	393.87
Northern Jiangsu	1,111 (21.39)	296.28[†, §]			233 (18.60)	175.19	380 (20.87)	275.49	498 (23.48)	478.59
Vaccine Type										
CRM197	2,576 (49.59)	286.69[¶]	76.13	<0.001[&]	605 (48.28)	196.23	853 (46.84)	275.11	1,118 (52.71)	399.04
TT	1,821 (35.05)	286.01[¶]			578 (46.13)	213.99	623 (34.21)	271.20	620 (29.23)	452.99
TT/DT	798 (15.36)	399.84			70 (5.59)	276.37	345 (18.95)	413.20	383 (18.06)	422.01
Dose										
1st dose	1,532 (29.49)	310.67[**, ††]	35.71	<0.001[&]	387 (30.89)	211.96	569 (31.25)	326.58	576 (27.16)	422.53
2nd dose	1,476 (28.41)	320.46[**, §§]			359 (28.65)	217.93	527 (28.94)	318.75	590 (27.82)	452.01
3rd dose	1,060 (20.40)	256.05			241 (19.23)	168.80	381 (20.92)	256.53	438 (20.65)	356.99
4th dose	1,127 (21.69)	307.01[††, §§]			266 (21.23)	234.05	344 (18.89)	254.48	517 (24.38)	437.19

Note: Southern Jiangsu: including Nanjing, Zhenjiang, Suzhou, Wuxi, Changzhou; Central Jiangsu: including Yangzhou, Taizhou, Nantong; Northern Jiangsu: including Xuzhou, Lianyungang, Huai'an, Yancheng, Suqian;

Total number of AEFI cases=5,195; The number of AEFI cases in 2022=1,253; The number of AEFI cases in 2023=1,821; The number of AEFI cases in 2024=2,121.

Abbreviation: AEFI=adverse events following immunization; PCV13=13-valent pneumococcal conjugate vaccine; RR=reporting rate (per 100,000 doses); CRM197=cross-reactive material 197; TT=tetanus toxoid; TT/DT=tetanus toxoid/diphtheria toxoid.

*, †, §, ¶, **, ††, §§ same superscript letters indicate no significant difference between the corresponding subgroups (*P*>0.05, Bonferroni correction);

[&] *P*<0.05.

(399.84 per 100,000 doses) was significantly higher than that for the CRM197-carrier (286.69 per 100,000 doses) and the TT-carrier (286.01 per 100,000 doses). Although a dual-carrier design may enhance immunogenicity, it may also increase reactogenicity. Animal studies have suggested that different carrier proteins elicit distinct T helper cell responses, potentially leading to carrier-induced epitopic suppression or synergistic enhancement (*8*). However, given that the TT/DT-carrier PCV13 was licensed only recently, its higher AEFI reporting rate may also be related to the Weber effect — a phenomenon in which new vaccines often experience elevated adverse event reporting rates shortly after market introduction, which then stabilize over time (*9*). Furthermore, the relatively small number of TT/DT-carrier vaccine doses administered in the present study (199,579 doses) suggests that the statistical stability of this finding needs to be confirmed with additional accumulated data. Of note, a

TABLE 3. Characteristics of AEFI RR after PCV13 in Jiangsu Province from 2022 to 2024.

Group	Common adverse reactions		Rare adverse reactions		Coincidental event	
	AEFI cases	RR (per 100,000 doses)	AEFI cases	RR (per 100,000 doses)	AEFI cases	RR (per 100,000 doses)
Age						
<1 year	3,450	279.82	32	2.60	26	2.11
1 year≤Age<2 years	1,460	314.12	16	3.44	15	3.23
2 years≤Age<3 years	47	253.01	1	5.38	0	0.00
≥3 years	146	944.43	1	6.47	1	6.47
Sex						
Male	2,826	314.84	33	3.68	23	2.56
Female	2,277	271.98	17	2.03	19	2.27
Region						
Southern Jiangsu	3,266	300.93	34	3.13	39	3.59
Central Jiangsu	741	269.92	3	1.09	1	0.36
Northern Jiangsu	1,096	292.28	13	3.47	2	0.53
Vaccine Type						
CRM197	2,519	280.35	30	3.34	27	3.00
TT	1,792	281.45	16	2.51	13	2.04
TT/DT	792	396.84	4	2.00	2	1.00
Dose						
1st dose	1,507	305.60	17	3.45	8	1.62
2nd dose	1,453	315.46	13	2.82	10	2.17
3rd dose	1,040	251.22	8	1.93	12	2.90
4th dose	1,103	300.47	12	3.27	12	3.27

Note: Southern Jiangsu: including Nanjing, Zhenjiang, Suzhou, Wuxi, Changzhou; Central Jiangsu: including Yangzhou, Taizhou, Nantong; Northern Jiangsu: including Xuzhou, Lianyungang, Huai'an, Yancheng, Suqian.
Abbreviation: AEFI=adverse events following immunization; PCV13=13-valent pneumococcal conjugate vaccine; RR=reporting rate (per 100,000 doses); CRM197=cross-reactive material 197; TT=tetanus toxoid; TT/DT=tetanus toxoid/diphtheria toxoid.

significant difference in AEFI reporting rates was observed between the CRM197-carrier and TT-carrier PCV13s, consistent with previous findings from Jiangsu Province (*4*) and multi-center findings (*10*). This further confirms the established safety profiles of these two conventional carrier-protein vaccines.

Age-stratified analysis revealed that the AEFI RR in children older than 3 years (3,829.48 per 100,000 doses) was significantly higher than that in other age groups, which differs from previous study results. A PCV13 surveillance study in Zhejiang Province reported the highest AEFI reporting rate in infants aged 6–11 months (*7*), and the Australian AusVax Safety system identified children aged 6 months to 4 years as a high-risk population for AEFIs (*11*). Although children older than 3 years had the highest AEFI RR in the present study, the majority of these events were mild common reactions, and the absolute reporting rate remained low and clinically acceptable. The higher relative rate in this age group is likely attributable to enhanced self-expression and greater guardian attention rather than a true increase in biological risk (*12–13*).

Fever, local redness, and local induration were the most frequently reported common adverse reactions, which is consistent with PCV13 safety studies conducted both domestically and internationally (*7,14*). Notably, the proportion of high-grade fever (≥ 38.6 °C) following vaccination with the TT-carrier and TT/DT-carrier PCV13s was higher than that with the CRM197-carrier PCV13, whereas the CRM197-carrier vaccine was predominantly associated with moderate-grade fever (37.6–38.5 °C). This difference may be related to variations in the cytokine profiles induced by different carrier proteins (*10*).

In the present study, DPA results showed that general reactions (fever, redness, and induration) exhibited strong positive signals across all four

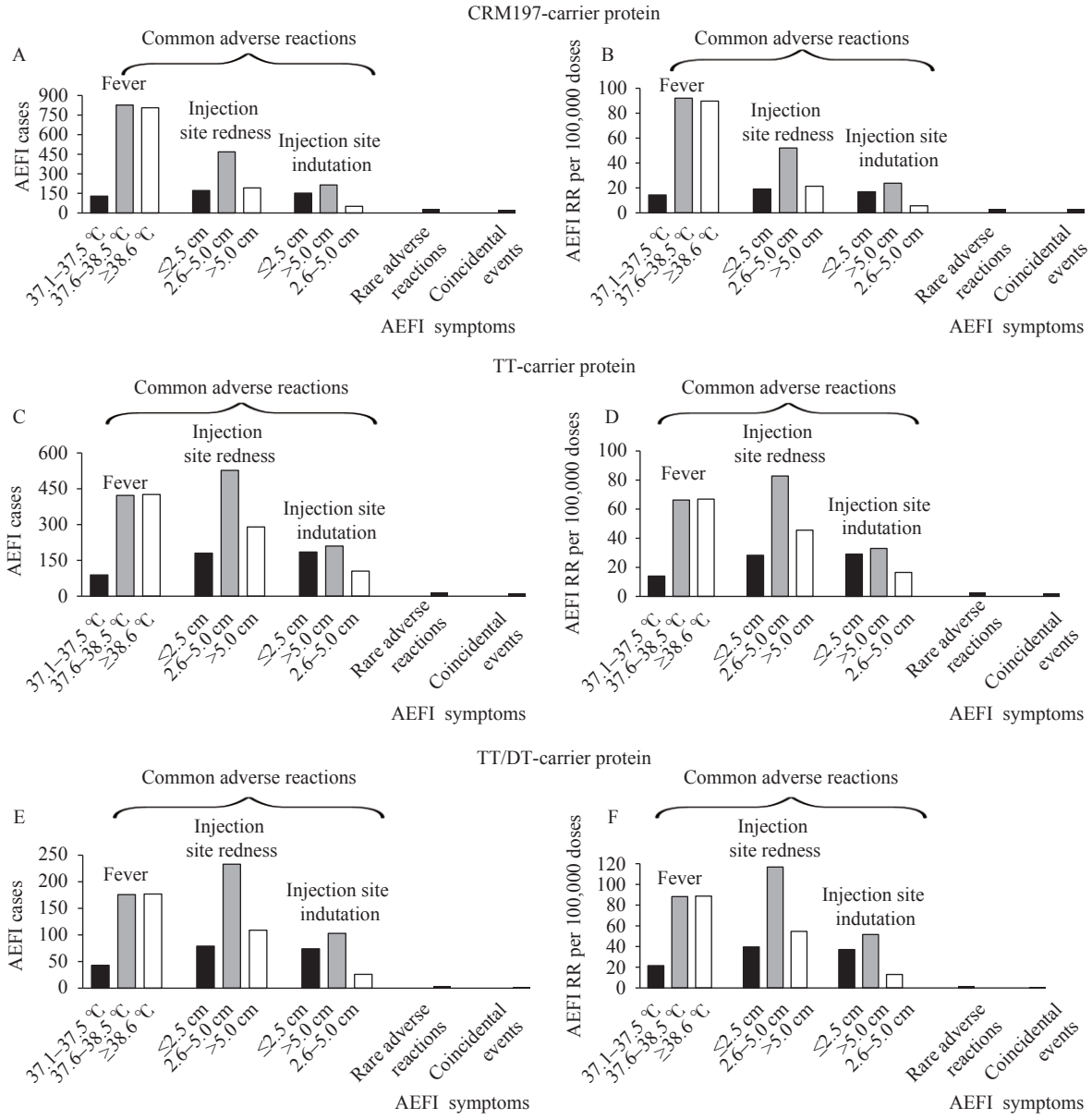

FIGURE 1. Distribution of AEFI cases (left panel) and RR per 100,000 doses (right panel) associated with PCV13 in Jiangsu Province from 2022 to 2024. (A) AEFI cases of CRM197 carrier protein. (B) AEFI RR per 100,000 doses of CRM197-carrier protein. (C) AEFI cases of TT-carrier protein. (D) AEFI RR per 100,000 doses of TT-carrier protein. (E) AEFI cases ofTT/DT-carrier protein. (F) AEFI RR per 100,000 doses of TT/DT-carrier protein.
Abbreviation: AEFI=adverse events following immunization; PCV13=13-valent pneumococcal conjugate vaccine; RR=reporting rate (per 100,000 doses); CRM197=cross-reactive material 197; TT=tetanus toxoid; TT/DT=tetanus toxoid/diphtheria toxoid.

methods, consistent with the known safety profile of PCV13 (*7*). Collectively, these results indicated that general reactions are AEFIs of particular concern following PCV13 vaccination. Subgroup analysis revealed a weak signal for allergic rash associated with the CRM197-carrier PCV13 under PRR/ROR, but this was not corroborated by BCPNN; the evidence remains inconclusive and hypothesis-generating, warranting continued attention. A previous study reported that CRM197, a non-toxic diphtheria toxin mutant, may induce IgE-mediated allergic reactions through cross-reactivity with human proteins (*15*). Vaccine Adverse Event Reporting System data show rash-reporting rates after PCV13 vaccination ranging from 0.6 to 2.3 per 100,000 doses, predominantly with CRM197-carrier products (*16*). However, the signal value in this study was close to the threshold, necessitating a comprehensive assessment in

TABLE 4. Disproportionality analysis of AEFI reports (clinical diagnosis) associated with PCV13 in Jiangsu Province from 2022 to 2024.

Diagnosis	RR (per 100,000 doses)	PRR-1.96SE	ROR-1.96SE	MHRA			BCPNN
				AEFI cases	PRR	χ^2	IC-2SD
General Reaction (Fever/Redness/Induration, etc.)	290.64	6.61	165.38	5,042	6.79	24912.69	2.72
Allergic Reactions-Allergic Purpura	0.06	0.00	0.00	1	0.00	740.14	−12.42
Allergic Reactions-Allergic Rash	4.15	0.08	0.07	72	0.10	605.13	−3.71
Allergic Reactions-Urticaria	0.98	0.01	0.01	17	0.02	708.53	−6.15
Febrile Seizures	0.12	0.00	0.00	2	0.00	738.15	−10.58
Thrombocytopenic Purpura	0.35	0.00	0.00	6	0.01	730.19	−8.13
Others	3.17	0.06	0.05	55	0.07	636.22	−4.14

Note: PRR: Proportional Reporting Ratio, the lower limit of the 95% two-sided confidence interval >1; ROR: Reporting Odds Ratio, the lower limit of the 95% two-sided confidence interval >1; MHRA: the Medicines and Healthcare Products Regulatory Agency method, the number of AEFI reports a≥3, PRR≥2 and χ^2≥4; BCPNN: Bayesian Confidence Propagation Neural Network method, the lower limit of the 95% two-sided confidence interval of the Information Component (IC) is greater than 0.
Abbreviation: AEFI=adverse events following immunization; PCV13=13-valent pneumococcal conjugate vaccine; RR=reporting rate (per 100,000 doses).

conjunction with clinical evaluation and subsequent surveillance data.

This study provides the first evidence for a post-marketing safety assessment of the new TT/DT-carrier PCV13. Some limitations should be acknowledged. This study used passive surveillance data, which has inherent limitations. For example, the vaccine safety awareness of the vaccinees or their guardians, as well as the completeness of reports by healthcare professionals, can affect the quality of reports. Passive surveillance only captures information from AEFI reporters; therefore, some conclusions in this study lack control groups. Further prospective active surveillance studies are warranted to confirm these results. Although the carrier protein type was the focus of this study, AEFI is a multifactorial outcome, and other factors, such as manufacturer-specific production processes, adjuvant formulation, and host characteristics, may also influence reactogenicity and should be addressed in future studies.

The findings indicate that AEFIs reported following administration of the three PCV13s with different carrier protein types in Jiangsu Province (2022–2024) were predominantly mild and fell within the category of common adverse reactions, which is broadly consistent with safety data from pre-licensure or post-licensure trials. These results may help alleviate parental concerns regarding the safety of the TT/DT dual-carrier PCV13 and improve vaccination coverage among children in China.

Acknowledgements: Gratitude goes to all staff members who participated in this study.

Conflicts of interest: No conflicts of interest.

Ethical statement: The research does not involve ethical review.

Funding: Supported by the Prevention and Control of Emerging and Major Infectious Diseases-National Science and Technology Major Project (2025ZD01902101).

doi: 10.46234/ccdcw2026.199

[#] Corresponding author: Jing Yu, yujing@jscdc.cn.

[1] Department of Expanded Program on Immunization, Jiangsu Provincial Center for Disease Control and Prevention (Jiangsu Provincial Academy of Preventive Medicine), Nanjing City, Jiangsu Province, China.

Copyright © 2026 by Chinese Center for Disease Control and Prevention & Chinese Academy of Preventive Medicine. All content is distributed under a Creative Commons Attribution Non Commercial License 4.0 (CC BY-NC).

Submitted: April 29, 2026
Accepted: September 24, 2026
Issued: October 02, 2026

REFERENCES

1. Peng R, Zhang T, Dunne EM, Xu ZY, Sun AL, Cheng JY, et al. Effectiveness and impact of 7 and 13-valent pneumococcal conjugate vaccines in Chinese children: a systematic review and meta-analysis. Hum Vaccin Immunother 2025;21(1):2573542. https://doi.org/10.1080/21645515.2025.2573542.
2. Wang SS, Li B, Chen Q, Wang CN, Wang B, Ye Q, et al. Pneumococcal vaccines in China. Hum Vaccin Immunother 2025;21(1):2460274. https://doi.org/10.1080/21645515.2025.2460274.
3. Zhang HN, Wang CF, Zhang HJ, Wahl B, Deloria Knoll M, Lai XZ, et al. Economic evaluation of childhood pneumococcal conjugate vaccination programs in Qinghai and Hainan provinces, China. Expert Rev Vaccines 2025;24(1):67 – 80. https://doi.org/10.1080/14760584.2024.2443223.
4. Hu R, Liu YB, Zhang L, Kang GD, Xu BR, Li MM, et al. Post-marketing safety surveillance for both CRM197 and TT carrier proteins

PCV13 in Jiangsu, China. Front Public Health 2023;11:1272562. https://doi.org/10.3389/fpubh.2023.1272562.
5. Syrogiannopoulos GA, Grivea IN, Moriondo M, Nieddu F, Michoula AN, Calabrese MR, et al. Molecular surveillance of pneumococcal carriage following completion of immunization with the 13-valent pneumococcal conjugate vaccine administered in a 3 + 1 schedule. Sci Rep 2021;11(1):24534. https://doi.org/10.1038/s41598-021-03720-y.
6. China NHCotPsRo. Circular on issuing the national guideline for the surveillance of adverse events following immunization (No.94 (2010) of the General Office of the Ministry of Health). 2010. https://www.nhc.gov.cn/jkj/c100063/201006/6c66bba9aa744e97bea8855d7350a481.shtml. [2026-4-29]. (In Chinese).
7. Hu Y, Pan XJ, Chen FX, Wang Y, Liang H, Shen LZ, et al. Surveillance of adverse events following immunization of 13-valent pneumococcal conjugate vaccine among infants, in Zhejiang province, China. Hum Vaccines Immunother 2022;18(1):2035141. https://doi.org/10.1080/21645515.2022.2035141.
8. Yu R, Xu JJ, Hu T, Chen W. The pneumococcal polysaccharide-tetanus toxin native C-Fragment conjugate vaccine: the carrier effect and immunogenicity. Mediat Inflamm 2020;2020:9596129. https://doi.org/10.1155/2020/9596129.
9. Wallenstein EJ, Fife D. Temporal patterns of NSAID spontaneous adverse event reports: the Weber effect revisited. Drug Safety 2001;24(3):233 – 7. https://doi.org/10.2165/00002018-200124030-00006.
10. Martinón-Torres F, Gimenez-Sanchez F, Gurtman A, Bernaola E, Diez-Domingo J, Carmona A, et al. 13-valent pneumococcal conjugate vaccine given with meningococcal C-tetanus toxoid conjugate and other routine pediatric vaccinations: immunogenicity and safety. Pediatr Infect Dis J 2012;31(4):392 – 9. https://doi.org/10.1097/INF.0b013e31824b972b.
11. Pillsbury AJ, Glover C, Jacoby P, Quinn HE, Fathima P, Cashman P, et al. Active surveillance of 2017 seasonal influenza vaccine safety: an observational cohort study of individuals aged 6 months and older in Australia. BMJ Open 2018;8(10):e023263. https://doi.org/10.1136/bmjopen-2018-023263.
12. Nicoli F, Mantelli B, Gallerani E, Telatin V, Squarzon L, Masiero S, et al. Effects of the age of vaccination on the humoral responses to a human papillomavirus vaccine. npj Vaccines 2022;7(1):37. https://doi.org/10.1038/s41541-022-00458-0.
13. Lopes SRC, Perin JLR, Prass TS, Carvalho SMD, Lessa SC, Dórea JG. Adverse events following immunization in Brazil: age of child and vaccine-associated risk analysis using logistic regression. Int J Environ Res Public Health 2018;15(6):1149. https://doi.org/10.3390/ijerph15061149.
14. Chevallier B, Vesikari T, Brzostek J, Knuf M, Bermal N, Aristegui J, et al. Safety and reactogenicity of the 10-valent pneumococcal non-typeable *Haemophilus influenzae* protein D conjugate vaccine (PHiD-CV) when coadministered with routine childhood vaccines. Pediatr Infect Dis J 2009;28(4):S109 – 18. https://doi.org/10.1097/INF.0b013e318199f62d.
15. Lyu SW, Su H, Yu FM, Wang QS, Guo YY, Li GY, et al. Therapeutic effect and mechanism of *Caulophyllum robustum* maxim extract on adjuvant arthritis rats. Tradit Chin Drug Res Clin Pharmacol 2017;28(2):164 – 71. https://doi.org/10.19378/j.issn.1003-9783.2017.02.005.
16. Shimabukuro TT, Nguyen M, Martin D, DeStefano F. Safety monitoring in the Vaccine Adverse Event Reporting System (VAERS). Vaccine 2015;33(36):4398 – 405. https://doi.org/10.1016/j.vaccine.2015.07.035.

SUPPLEMENTARY MATERIALS

Introduction to the Data Sources

The data used in this study have several advantages. First, the Jiangsu Province Vaccination Integrated Service Management Information System (JSEIRS) is an advanced system in the field of disease control in China, achieving multiple pioneering and unprecedented accomplishments. Data quality can be guaranteed, with the authenticity of individual vaccination records reaching 100% through full traceability using three pathways: electronic traceability code, vaccine lot number, and vaccine code. Second, the AEFI surveillance sensitivity in Jiangsu Province has consistently ranked among the highest in the country, exceeding 1 per 1,000 doses, which is far above the national requirement of 0.5 per 1,000 doses. Third, regarding the 13-valent pneumococcal conjugate vaccines with different carrier proteins, we began investigating differences in adverse reaction rates several years ago, as documented in relevant publications. Jiangsu Province has invested considerable time and effort in researching PCV13s with different carrier proteins. Unmatched records were returned to the local CDCs for verification. After confirming the reasons for non-matching, primarily missing or incorrect basic information, the records were corrected and included in the study.

Data Analysis for DPA

For each PCV13 type, we performed a separate disproportionality analysis. In each analysis, the target vaccine was defined as the specific PCV13 type under evaluation (CRM197-carrier, TT-carrier, or TT/DT-carrier). Control vaccines were defined as all other vaccines administered in Jiangsu Province during the same study period (January 2022 to December 2024), excluding the target PCV13 itself. However, because our study period included only three PCV13s and no other vaccine types were included in the AEFI reports relevant to PCV13, the control group for each target vaccine consisted of the remaining two PCV13 types (i.e., other PCV13s).

Usually, the positive signal markers for proportionality imbalance analysis are: 1) PRR: the lower limit of the 95% two-sided confidence interval >1; 2) ROR: the lower limit of the 95% two-sided confidence interval >1; 3) MHRA: the number of AEFI reports a ≥3, PRR ≥2 and $\chi^2 \geq 4$; 4) BCPNN: the lower limit of the 95% two-sided confidence interval of the Information Component (IC) is greater than 0. We applied the Haldane–Anscombe correction (adding 0.5 to all four cells) to calculate the PRR and ROR, preventing division by zero when b, c, or d equaled zero (*1*). For the MHRA method, no correction was used; a positive signal was considered only when the raw count a ≥3, regardless of the corrected values.

REFERENCES

1. Noguchi Y, Yoshizawa S, Aoyama K, Kubo S, Tachi T, Teramachi H. Verification of the "Upward Variation in the Reporting Odds Ratio Scores" to Detect the Signals of Drug-Drug Interactions. Pharmaceutics. 2021 Sep 22;13(10):1531. doi: 10.3390/pharmaceutics13101531. PMID: 34683823; PMCID: PMC8537362.

SUPPLEMENTARY TABLE S1. Symptoms and diagnostic characteristics of AEFI after PCV13 in Jiangsu Province, 2022–2024.

Group	CRM197-carrier protein		TT-carrier protein		TT/DT-carrier protein		Total	
	AEFI cases (%)	RR (per 100,000 doses)	AEFI cases (%)	RR (per 100,000 doses)	AEFI cases (%)	RR (per 100,000 doses)	AEFI cases (%)	RR (per 100,000 doses)
Common Adverse Reactions								
Fever (℃)								
37.1–37.5	129 (5.01)	14.36	89 (4.89)	13.98	43 (5.39)	21.55	261 (5.02)	15.04
37.6–38.5	827 (32.10)	92.04	422 (23.17)	66.28	176 (22.06)	88.19	1,425 (27.43)	82.14
≥38.6	806 (31.29)	89.70	426 (23.39)	66.91	177 (22.18)	88.69	1,409 (27.12)	81.22
Total	1,762 (68.40)	196.10	937 (51.46)	147.17	396 (49.62)	198.42	3,095 (59.58)	178.41
Redness (cm)								
≤2.5	172 (6.68)	19.14	180 (9.88)	28.27	79 (9.90)	39.58	431 (8.30)	24.84
2.6-5.0	468 (18.17)	52.08	527 (28.94)	82.77	233 (29.20)	116.75	1,228 (23.64)	70.79
>5.0	192 (7.45)	21.37	290 (15.93)	45.55	109 (13.66)	54.61	591 (11.38)	34.07
Total	832 (32.30)	92.60	997 (54.75)	156.59	421 (52.76)	210.94	2,250 (43.31)	129.70
Induration (cm)								
≤2.5	152 (5.90)	16.92	185 (10.16)	29.06	74 (9.27)	37.08	411 (7.91)	23.69
2.6-5.0	214 (8.31)	23.82	210 (11.53)	32.98	103 (12.91)	51.61	527 (10.14)	30.38
>5.0	51 (1.98)	5.68	105 (5.77)	16.49	26 (3.26)	13.03	182 (3.50)	10.49
Total	417 (16.19)	46.41	500 (27.46)	78.53	203 (25.44)	101.71	1,120 (21.56)	64.56
Other Symptoms								
Sweating	24 (0.93)	2.67	16 (0.88)	2.51	3 (0.38)	1.50	43 (0.83)	2.48
Nausea	1 (0.04)	0.11	3 (0.16)	0.47	1 (0.13)	0.50	5 (0.10)	0.29
Fatigue	100 (3.88)	11.13	84 (4.61)	13.19	32 (4.01)	16.03	216 (4.16)	12.45
Abdominal Pain	0 (0.00)	0.00	1 (0.05)	0.16	0 (0.00)	0.00	1 (0.02)	0.06
Diarrhea	47 (1.82)	5.23	19 (1.04)	2.98	13 (1.63)	6.51	79 (1.52)	4.55
Arthralgia	0 (0.00)	0.00	2 (0.11)	0.31	1 (0.13)	0.50	3 (0.06)	0.17
Cough	98 (3.80)	10.91	43 (2.36)	6.75	25 (3.13)	12.53	166 (3.20)	9.57
Myalgia	8 (0.31)	0.89	17 (0.93)	2.67	13 (1.63)	6.51	38 (0.73)	2.19
Rhinorrhea	34 (1.32)	3.78	16 (0.88)	2.51	6 (0.75)	3.01	56 (1.08)	3.23
Pallor	0 (0.00)	0.00	1 (0.05)	0.16	0 (0.00)	0.00	1 (0.02)	0.06
Vomiting	33 (1.28)	3.67	36 (1.98)	5.65	8 (1.00)	4.01	77 (1.48)	4.44
Rash	122 (4.74)	13.58	36 (1.98)	5.65	15 (1.88)	7.52	173 (3.33)	9.97
Itching	52 (2.02)	5.79	45 (2.47)	7.07	18 (2.26)	9.02	115 (2.21)	6.63
Poor Appetite	114 (4.43)	12.69	76 (4.17)	11.94	29 (3.63)	14.53	219 (4.22)	12.62
Drowsiness	75 (2.91)	8.35	35 (1.92)	5.50	16 (2.01)	8.02	126 (2.43)	7.26
Headache	2 (0.08)	0.22	0 (0.00)	0.00	5 (0.63)	2.51	7 (0.13)	0.40
Dizziness	0 (0.00)	0.00	0 (0.00)	0.00	2 (0.25)	1.00	2 (0.04)	0.12
Chest Tightness	0 (0.00)	0.00	0 (0.00)	0.00	1 (0.13)	0.50	1 (0.02)	0.06
Pharynx Redness	12 (0.47)	1.34	3 (0.16)	0.47	1 (0.13)	0.50	16 (0.31)	0.92
Others	22 (0.85)	2.45	26 (1.43)	4.08	8 (1.00)	4.01	56 (1.08)	3.23
Total	744 (28.88)	82.80	459 (25.21)	72.09	197 (24.69)	98.71	1,400 (26.95)	80.70

Note: Total number of AEFI cases=5,195; The number of AEFI cases from CRM197-Carrier Protein=2,576; The number of AEFI cases from TT-Carrier Protein=1,821; The number of AEFI cases from TT/DT-Carrier Protein=798.

Abbreviation: AEFI=adverse events following immunization; PCV13=13-valent pneumococcal conjugate vaccine; CRM197=cross-reactive material 197; TT=tetanus toxoid; TT/DT=tetanus toxoid/diphtheria toxoid; RR=reporting rate (per 100,000 doses).

SUPPLEMENTARY TABLE S2. Disproportionality analysis of AEFI reports (clinical diagnosis) associated with CRM197-carrier protein PCV13 in Jiangsu Province from 2022 to 2024.

Diagnosis	RR	PRR-1.96SE	ROR-1.96SE	MHRA			BCPNN
				AEFI cases	PRR	χ^2	IC-2SD
General Reaction (Fever/Redness/Induration etc.)	143.13	0.98	0.45	2,483	0.99	7.91	−0.07
Allergic Reactions-Allergic Purpura	0.06	0.12	0.12	1	Inf	1.02	−1.87
Allergic Reactions-Allergic rash	2.65	**1.11**	**1.11**	46	1.80	5.98	−0.06
Allergic Reactions-Urticaria	0.63	0.69	0.69	11	1.86	1.56	−0.49
Febrile Seizures	0.06	0.11	0.11	1	1.02	0.00	−2.87
Thrombocytopenic Purpura	0.23	0.39	0.39	4	2.03	0.70	−1.02
Others	1.73	0.72	0.72	30	1.22	0.55	−0.39

Note: PRR: Proportional Reporting Ratio, the lower limit of the 95% two-sided confidence interval >1; ROR: Reporting Odds Ratio, the lower limit of the 95% two-sided confidence interval >1; MHRA: the Medicines and Healthcare Products Regulatory Agency method, the number of AEFI reports a≥3, PRR≥2 and χ^2≥4; BCPNN: Bayesian Confidence Propagation Neural Network method, the lower limit of the 95% two-sided confidence interval of the Information Component (IC) is greater than 0.
Abbreviation: AEFI=adverse events following immunization; PCV13=13-valent pneumococcal conjugate vaccine; RR=reporting rate (per 100,000 doses); CRM197=cross-reactive material 197.

SUPPLEMENTARY TABLE S3. Disproportionality analysis of AEFI reports (clinical diagnosis) associated with TT-carrier protein PCV13 in Jiangsu Province from 2022 to 2024.

Diagnosis	RR	PRR-1.96SE	ROR-1.96SE	MHRA			BCPNN
				AEFI cases	PRR	χ^2	IC-2SD
General Reaction (Fever/Redness/Induration etc.)	102.60	**1.00**	**1.03**	1,780	1.01	4.72	−0.06
Allergic Reactions-Allergic Purpura	0.00	0.03	0.03	0	0.00	0.54	−
Allergic Reactions-Allergic rash	0.98	0.34	0.34	17	0.57	4.20	−1.27
Allergic Reactions-Urticaria	0.17	0.14	0.14	3	0.40	2.27	−2.66
Febrile Seizures	0.06	0.19	0.19	1	1.85	0.20	−2.37
Thrombocytopenic Purpura	0.12	0.22	0.22	2	0.93	0.01	−2.11
Others	1.04	0.53	0.52	18	0.90	0.13	−0.78

Note: PRR: Proportional Reporting Ratio, the lower limit of the 95% two-sided confidence interval >1; ROR: Reporting Odds Ratio, the lower limit of the 95% two-sided confidence interval >1; MHRA: the Medicines and Healthcare Products Regulatory Agency method, the number of AEFI reports a≥3, PRR≥2 and χ^2≥4; BCPNN: Bayesian Confidence Propagation Neural Network method, the lower limit of the 95% two-sided confidence interval of the Information Component (IC) is greater than 0.
Abbreviation: AEFI=adverse events following immunization; PCV13=13-valent pneumococcal conjugate vaccine; RR=reporting rate (per 100,000 doses); TT=tetanus toxoid.

SUPPLEMENTARY TABLE S4. Disproportionality analysis of AEFI reports (clinical diagnosis) associated with TT/DT-carrier protein PCV13 in Jiangsu Province from 2022 to 2024.

Diagnosis	RR	PRR-1.96SE	ROR-1.96SE	MHRA			BCPNN
				AEFI cases	PRR	χ^2	IC-2SD
General Reaction (Fever/Redness/Induration etc.)	44.90	0.99	0.78	779	1.01	1.05	−0.10
Allergic Reactions-Allergic Purpura	0.00	0.08	0.08	0	0.00	0.18	−
Allergic Reactions-Allergic rash	0.52	0.42	0.41	9	0.79	0.46	−1.26
Allergic Reactions-Urticaria	0.17	0.41	0.41	3	1.18	0.07	−1.47
Febrile Seizures	0.00	0.05	0.05	0	0.00	0.36	−
Thrombocytopenic Purpura	0.00	0.02	0.02	0	0.00	1.09	−
Others	0.40	0.40	0.39	7	0.80	0.30	−1.36

Note: PRR: Proportional Reporting Ratio, the lower limit of the 95% two-sided confidence interval >1; ROR: Reporting Odds Ratio, the lower limit of the 95% two-sided confidence interval >1; MHRA: the Medicines and Healthcare Products Regulatory Agency method, the number of AEFI reports a≥3, PRR≥2 and χ^2≥4; BCPNN: Bayesian Confidence Propagation Neural Network method, the lower limit of the 95% two-sided confidence interval of the Information Component (IC) is greater than 0.
Abbreviation: AEFI=adverse events following immunization; PCV13=13-valent pneumococcal conjugate vaccine; RR=reporting rate (per 100,000 doses); TT/DT=tetanus toxoid/diphtheria toxoid.

Preplanned Studies

Genomic Epidemiology and Antimicrobial Susceptibility of Human Brucellosis — Shenzhen City, Guangdong Province, China, 2005–2024

Li Yuan[1,&]; Cong Niu[2,&]; Shiting Chen[3,&]; Qiongcheng Chen[2]; Shuang Wu[2]; Wenkai Cui[1]; Jianguang Cai[4]; Xiaolu Shi[2,#]

Summary

What is already known about this topic?

Brucellosis is a zoonotic disease historically concentrated in pastoral regions of China; however, an increasing number of cases have been reported in large urban centers in recent years.

What is added by this report?

Analysis of 191 human-derived Brucella isolates collected in Shenzhen between 2005 and 2024 showed that Brucella melitensis predominated and that Shenzhen isolates were interspersed with strains from multiple provinces, suggesting repeated introductions from other regions. Most cases occurred in working-age adults, and both imported cases and Shenzhen-resident cases without documented external exposure were identified.

What are the implications for public health practice?

These findings suggest that brucellosis control in highly urbanized settings should prioritize surveillance for imported infections, improved traceability and regulation of animal-derived food products, targeted protection of high-risk occupational groups, and continued genomic and antimicrobial susceptibility surveillance.

ABSTRACT

Introduction: Brucellosis is increasingly reported in highly urbanized areas of China. This study characterized the genomic epidemiology and antimicrobial susceptibility of human-derived *Brucella* isolates from Shenzhen, China.

Methods: We analyzed 191 culture-confirmed human *Brucella* isolates collected in Shenzhen between 2005 and 2024. Epidemiological data were obtained from routine investigations. Whole-genome sequencing was used for species identification, phylogenetic analysis, and core genome multilocus sequence typing (cgMLST). Antimicrobial susceptibility was assessed using broth microdilution, and temporal trends in the minimum inhibitory concentration (MIC) were evaluated using the Spearman rank correlation coefficient.

Results: *Brucella melitensis* was the predominant species (94.8%, 181/191). The isolates were distributed across multiple genetic clusters and interspersed with strains from several provinces, suggesting repeated introductions from other regions. Most isolates showed relatively low MIC values for commonly used first-line agents; however, some isolates had elevated rifampicin MIC values. Over the study period significant increases in the MIC were observed for levofloxacin, rifampicin, doxycycline, trimethoprim-sulfamethoxazole, ceftriaxone, ampicillin, and amikacin.

Conclusions: Interventions to improve brucellosis control in Shenzhen should focus on strengthening surveillance for imported infections, improving traceability of animal-derived food products, protecting high-risk occupational groups, and ongoing genomic and antimicrobial susceptibility monitoring.

Brucellosis is a globally important zoonotic disease caused by bacteria of the genus *Brucella* and remains a persistent public health concern despite long-standing control efforts (*1*). Human infection typically occurs through occupational exposure or consumption of contaminated animal-derived products, particularly unpasteurized dairy products (*2*). Although historically associated with pastoral and agricultural regions, brucellosis has increasingly been reported in large metropolitan areas, reflecting increased population mobility and changes in food distribution systems (*3*).

Shenzhen is a highly urbanized megacity

Copyright © 2026 by Chinese Center for Disease Control and Prevention

characterized by a large migrant population and extensive inter-regional movement of animal-derived food products. These features create conditions that may facilitate repeated introduction of *Brucella* from diverse geographic sources. However, genomic evidence describing the transmission dynamics and antimicrobial susceptibility patterns of human *Brucella* isolates in urban settings remains limited (*4*). This study aimed to characterize the genomic epidemiology and antimicrobial susceptibility profiles of human-derived Brucella isolates collected in Shenzhen over a 20-year period.

A total of 191 human-derived Brucella isolates recovered from culture-confirmed cases in Shenzhen between 2005 and 2024 were included in this study. Isolates were collected through the municipal brucellosis surveillance system, in which specimens from individuals with suspected brucellosis and Brucella-positive cultures identified by sentinel surveillance hospitals were referred to the Shenzhen Center for Disease Control and Prevention for laboratory confirmation, strain preservation, and epidemiological investigation. Demographic and epidemiological information, including age, sex, occupation, place of residence, date of onset, and exposure history, were extracted from routine case investigation records. Imported cases were defined as cases with epidemiological evidence indicating that exposure occurred outside Shenzhen, including cases with exposure in other provinces or other cities within Guangdong Province. Cases among Shenzhen residents without documented external exposure during the relevant exposure period were defined as cases without epidemiological evidence of infection acquired outside the city. As inclusion depended on successful culture confirmation and isolate availability, the isolates represented a convenience sample of available isolates rather than a random sample of all reported cases. Accordingly, the findings should be interpreted as isolate-based surveillance results rather than as a population-based representation of all reported cases.

Whole-genome sequencing was performed on the Illumina NovaSeq platform using paired-end 150-bp reads. Raw reads were filtered using Trimmomatic and assessed using FastQC. Species identification was initially performed using Kraken2 and was subsequently cross-checked against the phylogenetic placement and genome-based characteristics of representative *Brucella* reference strains. Draft assemblies were generated using SPAdes and evaluated for completeness, contamination, and structure using QUAST and CheckM. Core-genome single-nucleotide polymorphism (SNP) calling was conducted using Snippy, recombination regions were removed using Gubbins, and a maximum-likelihood phylogeny was reconstructed using FastTree. Core genome multilocus sequence typing (cgMLST) analysis was performed using SeqSphere+ to infer allelic relationships and construct minimum spanning trees (*5*).

Antimicrobial susceptibility testing was performed using the broth microdilution method. The minimum inhibitory concentration (MIC) values were interpreted according to the available clinical breakpoints or summarized using MIC distributions when *Brucella*-specific breakpoints were unavailable. For antimicrobial agents without available breakpoints, the MIC values were analyzed as continuous variables and temporal trends in MIC values were assessed using Spearman rank correlation analysis. For antimicrobial agents with available clinical breakpoints, categorical susceptibility outcomes were summarized descriptively and were not subjected to formal temporal trend testing. Statistical analyses were performed using R software (version 4.3.0; The R Foundation for Statistical Computing, Vienna, Austria), and two-sided P values <0.05 were considered statistically significant.

The annual number of culture-confirmed human Brucella isolates fluctuated during the study period, with a marked increase after 2013 and a peak in 2019 (n=37), followed by a drop in 2020. Between 2021 and 2024, the annual number of isolates remained below the 2019 peak (Figure 1A).

Most of the cases of human brucellosis were in adults of working age, with the majority of cases occurring in men (Figure 1B). Among individuals with available information, 68.4% (119/174) were male and 60.0% (102/170) were aged 25–54 years. The distribution of occupations was heterogeneous, with homemakers and unemployed individuals constituting the largest category, followed by food service workers, laborers, and business service workers (Figure 1C). Cases occurred among Shenzhen residents without documented external exposure but some imported cases were identified, reflecting Shenzhen's high population mobility and frequent interregional movement. The high proportion of cases occurred among individuals without traditional occupational exposure, suggesting that the epidemiological pattern of human brucellosis is changing in the Shenzhen urban setting.

The epidemiological sources and geographic distribution of cases are summarized in Figure 2.

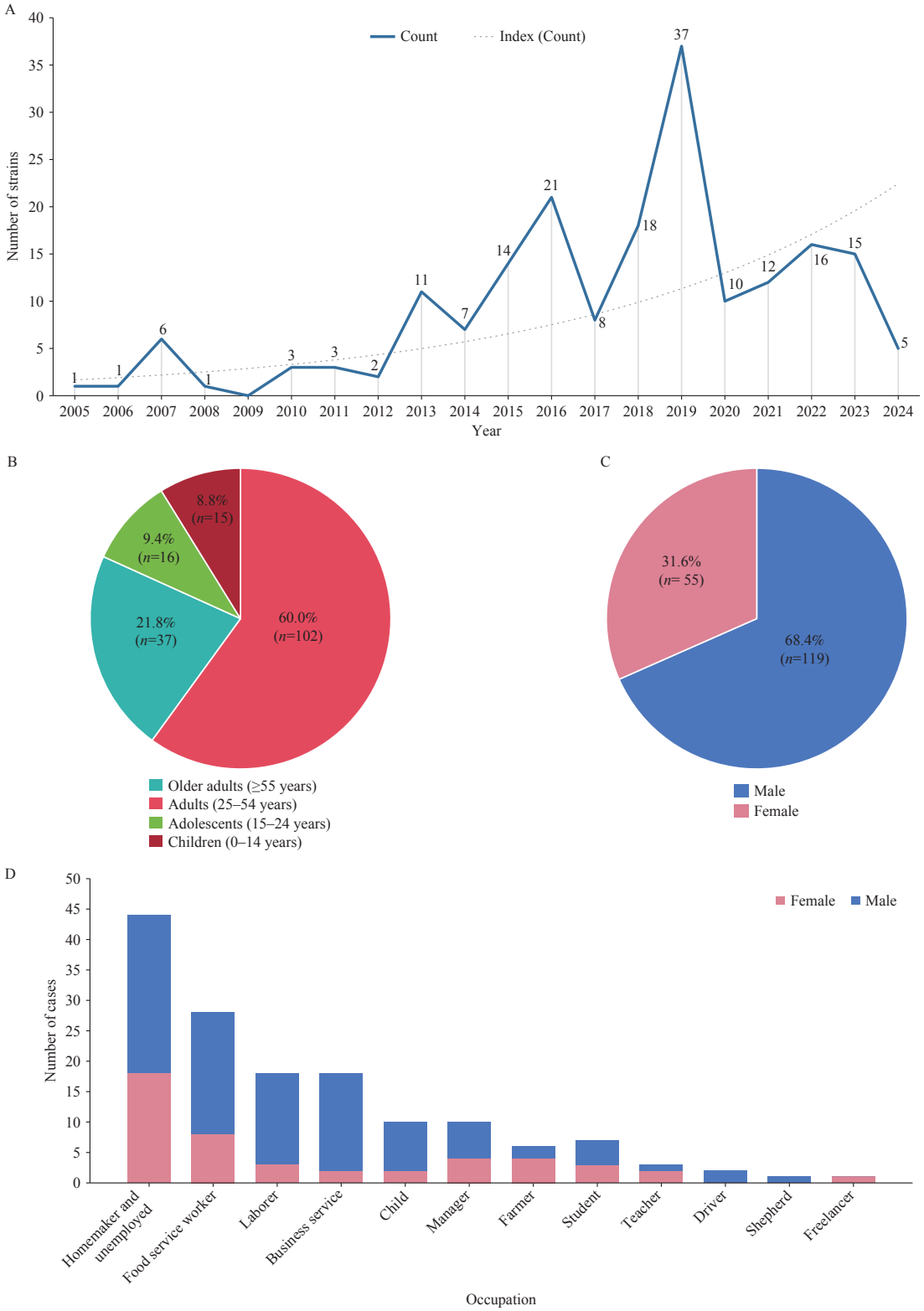

FIGURE 1. Temporal and demographic characteristics of human brucellosis cases in Shenzhen, 2005–2024. (A) Annual distribution of culture-confirmed human *Brucella* isolates collected in Shenzhen, 2005–2024. (B) Age distributions of human brucellosis among 170 cases with known age in Shenzhen. (C) Sex distributions of human brucellosis among 174 cases with known sex in Shenzhen. (D) Occupational distribution of human brucellosis cases in Shenzhen.

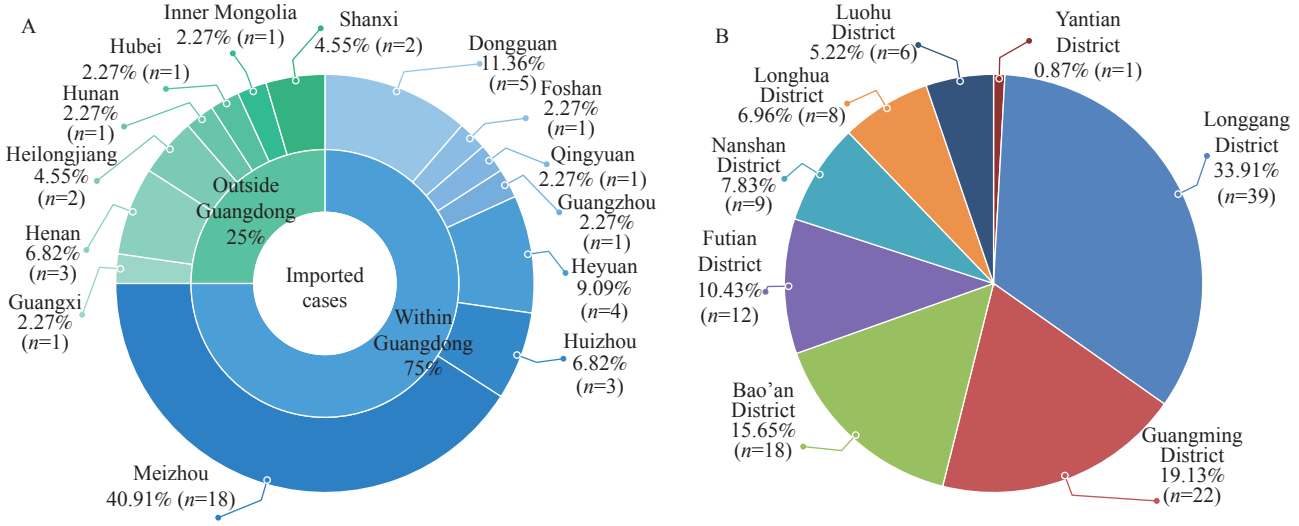

FIGURE 2. Epidemiological sources of human brucellosis cases associated with Shenzhen, China, 2005–2024. (A) Geographic origins of imported cases, including cases originating from within Guangdong Province and from other provinces of China. (B) District distribution of Shenzhen-resident cases without documented external exposure.

Among cases with available geographic information, Guangdong Province accounted for the majority of cases (*n*=148), followed by Henan (*n*=3), Heilongjiang and Shanxi (*n*=2 each), with Guangxi, Hunan, Hubei, and Inner Mongolia each contributing one case (Figure 3A). Of the 148 cases thought to be acquired within Guangdong Province, Shenzhen accounted for 115 cases (77.7%), followed by Meizhou (*n*=18), Dongguan (*n*=5), Heyuan (*n*=4), and Huizhou (*n*=3), with Guangzhou, Foshan, and Qingyuan each contributing one case (Figure 3B). Among the 115 cases thought to be acquired within Shenzhen, the highest number of cases was from Longgang District (*n*=39), followed by Guangming (*n*=22), Bao'an (*n*=18), Futian (*n*=12), Nanshan (*n*=9), Longhua (*n*=8), Luohu (*n*=6), and Yantian (*n*=1) (Figure 3C).

Genomic analysis showed that 181 of the 191 isolates (94.8%) were *Brucella melitensis*, followed by *Brucella abortus* (6 cases, 3.1%) and *Brucella suis* (4 cases, 2.1%). Core-genome SNP-based phylogenetic analysis of all human-derived *Brucella* isolates from Shenzhen revealed that the isolates were distributed across multiple major lineages and did not fit within a single localized clade (Figure 4A). Most Shenzhen isolates clustered closely with strains from other provinces, including Xinjiang, Inner Mongolia, Jiangxi, and Hainan, indicating close genomic relationships and suggesting repeated introductions from other provinces.

As *B. melitensis* accounted for the majority of isolates, an additional species-specific phylogenetic analysis was performed on *B. melitensis* isolates (Figure 4B). The *B. melitensis*-only tree showed that Shenzhen isolates were distributed mainly within the East Mediterranean lineage and were interspersed with strains from multiple domestic and international sources, suggesting repeated introductions from other regions, rather than expansion of a single local clone.

CgMLST-based minimum spanning tree analysis revealed consistent clustering patterns, with Shenzhen isolates embedded within broader genetic clusters containing isolates from multiple regions of China (Figure 4C). The predominance of *B. melitensis* among the isolates was consistent with previously reported epidemiological patterns in China. The detection of *B. abortus* and *B. suis* suggests that human infections in Shenzhen may be associated with multiple animal sources.

Antimicrobial susceptibility testing showed heterogeneous MIC distributions among isolates (Figure 5). Most isolates had relatively low MIC values for doxycycline, tetracycline, and trimethoprim-sulfamethoxazole. In contrast, some isolates had relatively high rifampicin MIC values.

Spearman rank correlation analysis showed statistically significant increases in the MIC values over time for levofloxacin (ρ =0.213, *P*=0.004), rifampicin (ρ =0.231, *P*<0.001), doxycycline (ρ =0.192, *P*=0.010), trimethoprim-sulfamethoxazole (ρ =0.274, *P*<0.001), ceftriaxone (ρ =0.162, *P*=0.026), ampicillin (ρ =0.241, *P*<0.001), and amikacin (ρ =0.253, *P*<0.001) (Table 1). No significant temporal trends were observed for erythromycin, streptomycin, tetracycline, ciprofloxacin, or gentamicin. Although

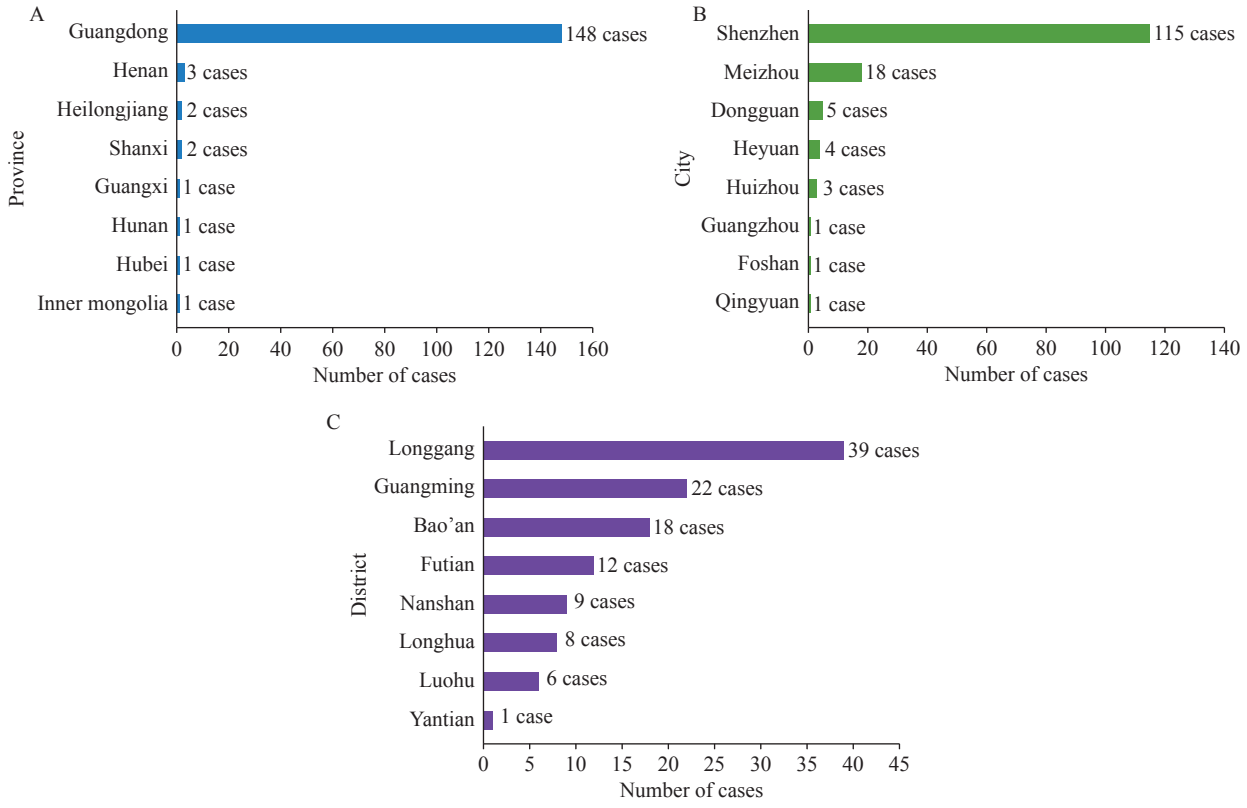

FIGURE 3. (A) Number of cases according to province of origin. (B) Number of cases according to city-level geographic origin within Guangdong Province. (C) Distribution of Shenzhen-resident cases without documented external exposure by district.

relatively low MIC values against recommended first-line agents were observed for most isolates, continued monitoring of temporal MIC trends is warranted.

DISCUSSION

This study provides a genomic and phenotypic overview of human-derived *Brucella* isolates collected in Shenzhen over two decades from 2005 to 2024. Combined phylogenetic and cgMLST analyses showed that Shenzhen isolates were genetically interspersed with isolates from multiple regions, suggesting repeated introductions from other geographic regions, rather than expansion of a single Shenzhen-specific lineage. These findings are consistent with the high population mobility in Shenzhen and extensive circulation of animal-derived food products.

The predominance of *B. melitensis*, together with its close genetic relationships to strains from multiple provinces, highlights the importance of inter-regional population movement and broader geographic mixing in shaping the epidemiology of urban brucellosis (*6*). The identification of *B. abortus* and *B. suis* further indicates that multiple animal reservoirs may contribute to human infection in this setting.

The occupational distribution of human brucellosis cases in Shenzhen was heterogeneous, indicating that urban brucellosis is not confined to traditional livestock-related occupations. Food service workers and other individuals involved in handling animal-derived products may face occupational or food-related exposure, whereas cases among homemakers, unemployed individuals, and other groups without traditional occupational exposure suggest that nonoccupational exposure pathways should also be considered. Contaminated animal-derived food products are an important potential source of exposure and pathogen introduction in Shenzhen, a megacity with complex food supply chains. These findings suggest that prevention strategies need to combine occupational protection, food safety supervision, public health education, and source tracing of high-risk animal products.

Most isolates were susceptible to recommended first-line agents (*7*). Recommended treatment regimens for human brucellosis commonly include doxycycline-based combination therapy, particularly doxycycline

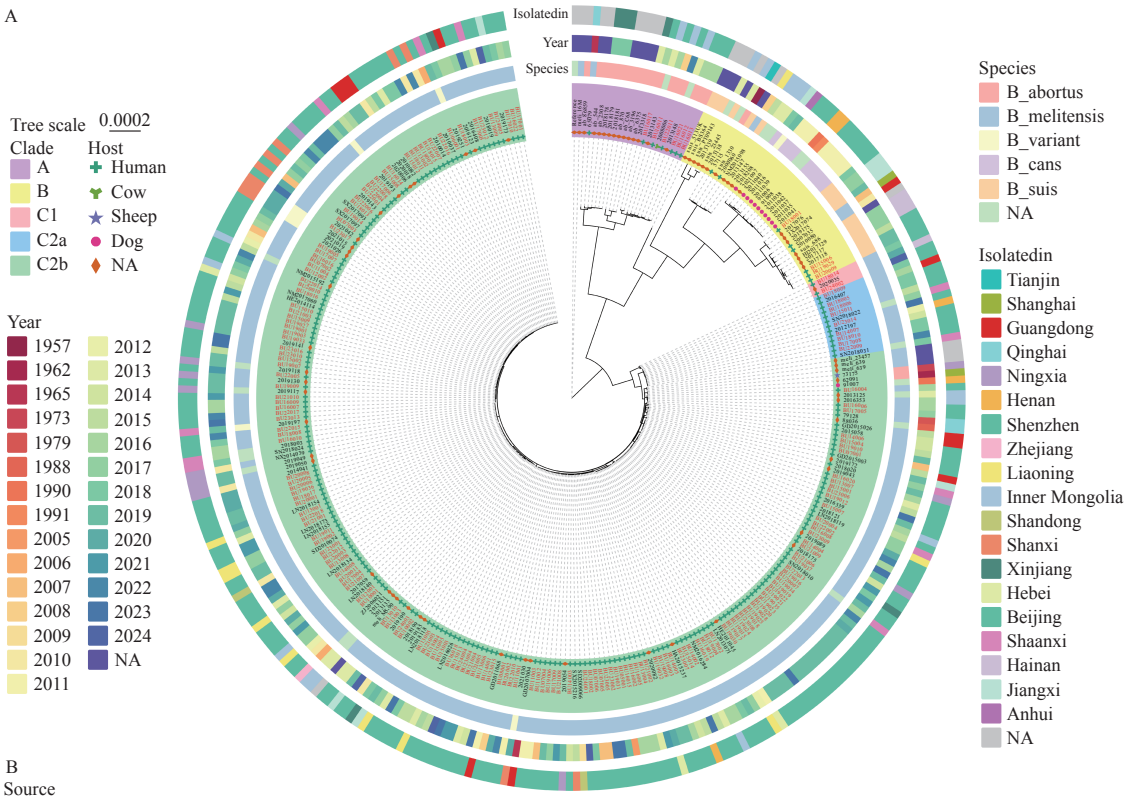
A
Isolatedin
Year
Species
Tree scale 0.0002
Clade
A
B
C1
C2a
C2b
Host
Human
Cow
Sheep
Dog
NA
Year
1957
1962
1965
1973
1979
1988
1990
1991
2005
2006
2007
2008
2009
2010
2011
2012
2013
2014
2015
2016
2017
2018
2019
2020
2021
2022
2023
2024
NA
Species
B_abortus
B_melitensis
B_variant
B_cans
B_suis
NA
Isolatedin
Tianjin
Shanghai
Guangdong
Qinghai
Ningxia
Henan
Shenzhen
Zhejiang
Liaoning
Inner Mongolia
Shandong
Shanxi
Xinjiang
Hebei
Beijing
Shaanxi
Hainan
Jiangxi
Anhui
NA

B
Source
Shenzhen
China
Malta
Argentina
Portugal
Somalia
Pakistan
Zimbabwe
UnitedKingdom
Russia
Reference
Malaysia
USA
Egypt
Kuwait
Canada
Georgia
Afghanistan
Albania
Iran
Iraq
Morocco
Turkmenistan
Turkey
Bulgaria
Syria
India
SaudiArabia
Italy
Norway
France
Lineage
WestMediterranean
USA
African
EastMediterranean
BAPS
BAPS1
BAPS2
BAPS3
BAPS4
BAPS5
BAPS6
BAPS7
Host
Human
Cattle
Ovisaries
Goat
Sheep
NA
Bovine
Yak
none
bovine
Bostaurus
Ovisaries/Capra
Tree scale: 0.0001
Host
Source
BAPS

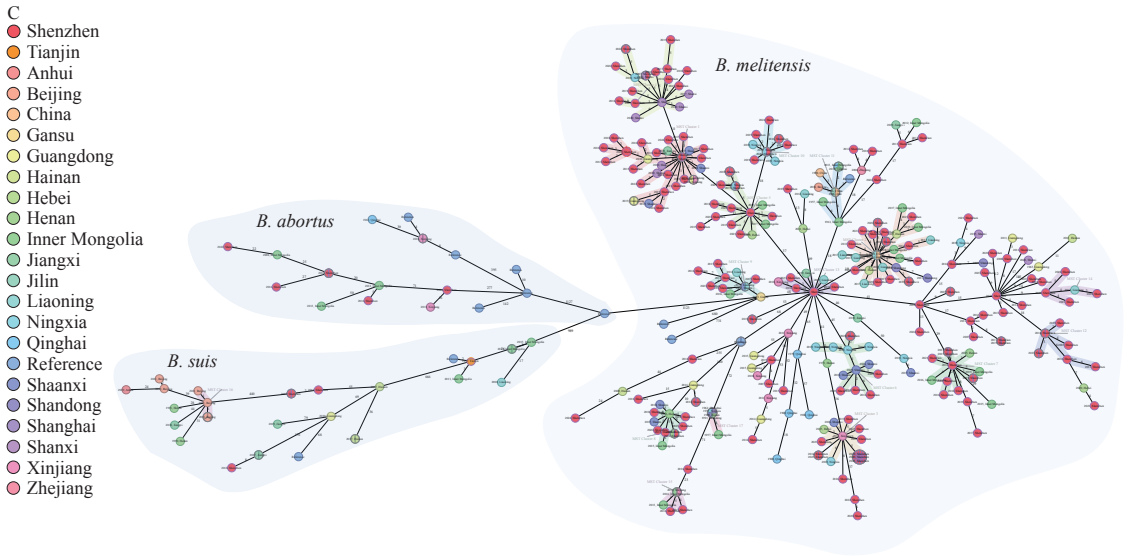

FIGURE 4. Phylogenetic structure and cgMLST-based relationships of human-derived *Brucella* isolates from Shenzhen and reference strains from China and other regions. (A) Maximum-likelihood phylogenetic tree constructed using non-recombinant core-genome single-nucleotide polymorphisms (SNPs), annotated by host, sampling year, species, and suspected geographic origin. (B) Species-specific maximum-likelihood phylogenetic tree of *Brucella melitensis* genomes from Shenzhen and representative reference strains, annotated by host, source, lineage, and Bayesian Analysis of Population Structure (BAPS) grouping. (C) Minimum-spanning tree based on core-genome multilocus sequence typing (cgMLST) allelic profiles, showing genetic relationships among Shenzhen isolates and representative *Brucella* reference strains from different species and geographic regions.
Note: Panel A provides an overview of the phylogenetic structure of the full isolate collection. Because *B. melitensis* accounted for the majority of Shenzhen isolates, panel B presents an additional species-specific phylogenetic analysis. Shenzhen *B. melitensis* isolates were mainly distributed within the East Mediterranean lineage and were interspersed with strains from multiple domestic and international sources, supporting repeated inter-regional introductions rather than expansion of a single local clone. Panel C shows that Shenzhen isolates were distributed within broader genetic clusters containing isolates from multiple regions of China.
Abbreviation: BAPS=bayesian analysis of population structure; cgMLST=core-genome multilocus sequence typing; SNP=single-nucleotide polymorphism.

plus rifampicin, although doxycycline plus streptomycin remains another standard option. In this study, most isolates had low doxycycline MIC values despite an increase in the values over time, whereas some isolates showed relatively high rifampicin MIC values. These findings indicate a need for ongoing local antimicrobial susceptibility surveillance to inform treatment decisions and detect emerging reductions in susceptibility (*8*). The MICs for levofloxacin, rifampicin, doxycycline, trimethoprim-sulfamethoxazole, ceftriaxone, ampicillin, and amikacin, increased significantly over time, whereas no significant temporal trends were detected for erythromycin, streptomycin, tetracycline, ciprofloxacin, or gentamicin (*9*). These findings do not indicate widespread clinical resistance but instead indicate that temporal MIC shifts and possible reductions in susceptibility require careful monitoring (*10*).

This study has several limitations. First, because the study was restricted to culture-confirmed isolates and inclusion depended on isolate availability, the analyzed strains may not reflect the full epidemiological spectrum of reported brucellosis cases in Shenzhen, particularly cases without microbiological confirmation; therefore, the possibility of selection bias cannot be excluded. Second, incomplete epidemiological information, including missing month-level onset data for some cases, limited seasonal analysis and the detailed reconstruction of transmission routes and exposure settings. Third, for several antimicrobial agents, the absence of standardized *Brucella*-specific clinical breakpoints required interpretation based primarily on the MIC distributions, which may limit comparability with other studies. Finally, data collection ended in 2024 because complete genomic and phenotypic datasets for more recent isolates were not available at the time of analysis; this may affect the timeliness of the findings.

In a highly urbanized city such as Shenzhen,

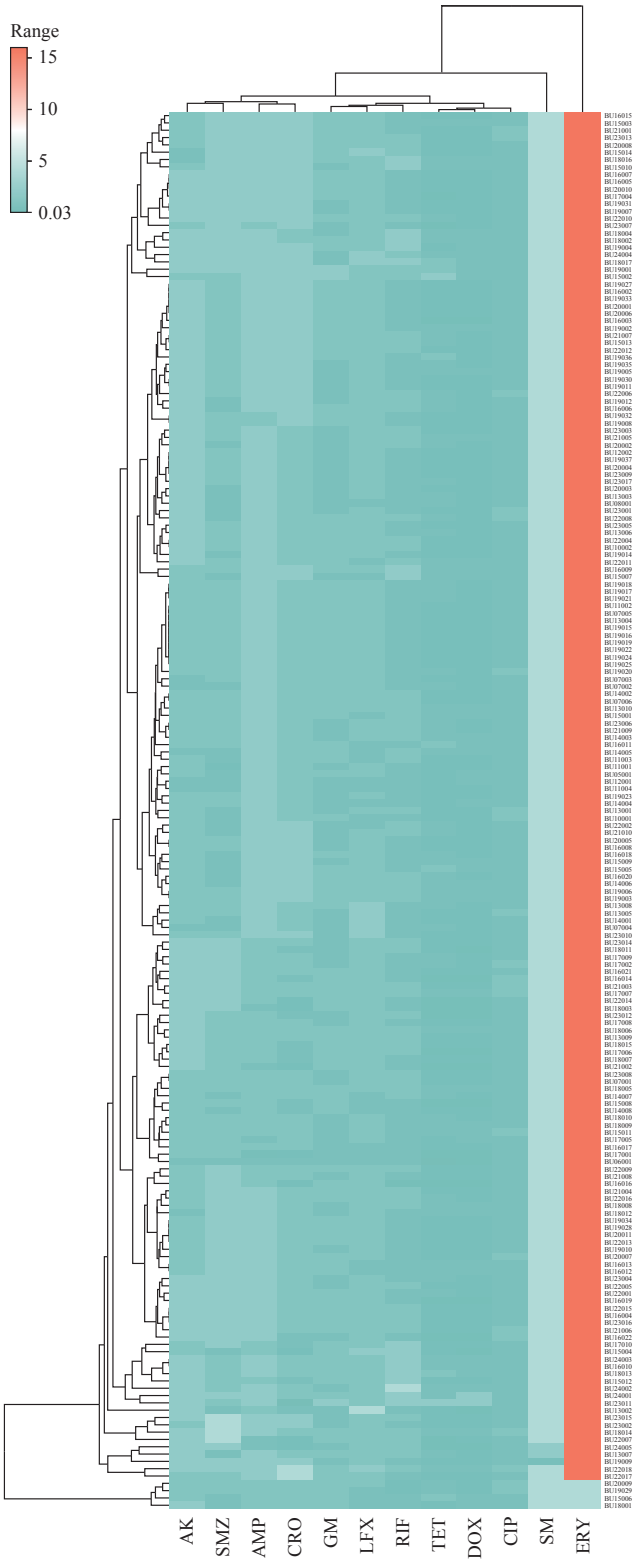

FIGURE 5. Antimicrobial susceptibility profiles of human-derived *Brucella* isolates from Shenzhen.
Note: Heatmap showing the minimum inhibitory concentration (MIC) distributions of the antimicrobial agents tested against human-derived *Brucella* isolates. The heatmap illustrates the heterogeneity of MIC distributions across isolates and antimicrobial agents.
Abbreviation: AK=amikacin; AMP=ampicillin; CIP=ciprofloxacin; CRO=ceftriaxone; DOX=doxycycline; ERY=erythromycin; GM=gentamicin; LFX=levofloxacin; MIC=minimum inhibitory concentration; RIF=rifampicin; SM=streptomycin; SMZ=trimethoprim-sulfamethoxazole; TET=tetracycline.

TABLE 1. Temporal trends in MIC values of antimicrobial agents among *Brucella* isolates from Shenzhen, 2005–2024, assessed using Spearman rank correlation analysis.

Antimicrobial agent	ρ	*P*
ERY	0.004	0.968
LFX	0.213	0.004
RIF	0.231	<0.001
DOX	0.192	0.010
SM	0.061	0.426
SMZ	0.274	<0.001
TET	0.134	0.077
CIP	0.052	0.512
CRO	0.162	0.026
GM	0.121	0.095
AMP	0.241	<0.001
AK	0.253	<0.001

Note: Significant positive temporal trends were observed in the MIC values for levofloxacin, rifampicin, doxycycline, trimethoprim-sulfamethoxazole, ceftriaxone, ampicillin, and amikacin ($P<0.05$). No significant temporal trends were observed for erythromycin, streptomycin, tetracycline, ciprofloxacin, or gentamicin.
Abbreviation: ρ=Spearman rank correlation coefficient (rho); AK=amikacin; AMP=ampicillin; CIP=ciprofloxacin; CRO=ceftriaxone; DOX=doxycycline; ERY=erythromycin; GM=gentamicin; LFX=levofloxacin; MIC=minimum inhibitory concentration; RIF=rifampicin; SM=streptomycin; SMZ=trimethoprim-sulfamethoxazole; TET=tetracycline.

brucellosis control should not rely solely on traditional assumptions of pastoral exposure. The findings of this study suggest that prevention strategies should include strengthened surveillance for imported infections, tighter supervision of animal-derived food products and maintaining traceability of their geographic origin, and targeted protection for food service workers and other occupational groups involved in handling, processing, transporting, or selling of animal-derived products. In addition, integration of whole-genome sequencing into routine surveillance could improve the identification of imported strains and support timely source tracing, whereas ongoing antimicrobial susceptibility monitoring may help with early detection of reduced susceptibility among circulating strains.

Acknowledgments: The authors thank the staff of the Shenzhen Center for Disease Control and Prevention and participating sentinel hospitals for their contributions to case surveillance, epidemiological investigation, isolate collection, laboratory testing, and strain preservation. We also acknowledge the researchers who generated and deposited the publicly available genome sequences used in the comparative genomic analyses.

Conflicts of interest: No conflicts of interest.

Ethical statement: This study was conducted as part of routine public health surveillance. All data were collected and analyzed in accordance with relevant institutional and national regulations. The study was exempt from institutional ethical review.

Funding: This study was supported in part by grants from the Shenzhen Science and Technology Program (SGDX20240115113259001), the Shenzhen Medical Research Fund (B2404002), the Shenzhen Key Laboratory for Surveillance of Major Infectious Diseases (SYSPG20241211173921049), and the Sanming Project of Medicine in Shenzhen (SZSM202211023). We also thank the affiliated institutions and research teams for their support and help.

doi: 10.46234/ccdcw2026.200

[#] Corresponding author: Xiaolu Shi, shixl@wjw.sz.gov.cn.

[1] School of Public Health, University of South China, Hengyang City, Hunan Province, China; [2] Shenzhen Center for Disease Control and Prevention, Shenzhen City, Guangdong Province, China; [3] School of Public Health, Shanxi Medical University, Taiyuan City, Shanxi Province, China; [4] School of Public Health, Southern Medical University, Guangzhou City, Guangdong Province, China.
[&] Joint first authors.

Copyright © 2026 by Chinese Center for Disease Control and Prevention & Chinese Academy of Preventive Medicine. All content is distributed under a Creative Commons Attribution Non Commercial License 4.0 (CC BY-NC).

Submitted: June 18, 2026
Accepted: August 06, 2026
Issued: October 02, 2026

REFERENCES

1. Pappas G, Papadimitriou P, Akritidis N, Christou L, Tsianos EV. The new global map of human brucellosis. Lancet Infect Dis 2006;6(2):91 – 9. https://doi.org/10.1016/S1473-3099(06)70382-6.
2. Franco MP, Mulder M, Gilman RH, Smits HL. Human brucellosis. Lancet Infect Dis 2007;7(12):775 – 86. https://doi.org/10.1016/S1473-3099(07)70286-4.
3. Lai SJ, Zhou H, Xiong WY, Yu HJ, Huang ZJ, Yu JX, et al. Changing epidemiology of human brucellosis, China, 1955-2014. Emerg Infect Dis 2017;23(2):184 – 94. https://doi.org/10.3201/eid2302.151710.
4. Whatmore AM, Koylass MS, Muchowski J, Edwards-Smallbone J, Gopaul KK, Perrett LL. Extended multilocus sequence analysis to describe the global population structure of the genus *Brucella*: Phylogeography and relationship to biovars. Front Microbiol 2016;7:2049. https://doi.org/10.3389/fmicb.2016.02049.
5. Janowicz A, De Massis F, Ancora M, Cammà C, Patavino C, Battisti A, et al. Core genome multilocus sequence typing and single nucleotide polymorphism analysis in the epidemiology of *Brucella melitensis* infections. J Clin Microbiol 2018;56(9):e00517 – 18. https://doi.org/10.1128/JCM.00517-18.
6. Tan KK, Tan YC, Chang LY, Lee KW, Nore SS, Yee WY, et al. Full genome SNP-based phylogenetic analysis reveals the origin and global

spread of *Brucella melitensis*. BMC Genomics 2015;16(1):93. https://doi.org/10.1186/s12864-015-1294-x.
7. Liu ZG, Di DD, Wang M, Liu RH, Zhao HY, Piao DR, et al. In vitro antimicrobial susceptibility testing of human *Brucella melitensis* isolates from Ulanqab of Inner Mongolia, China. BMC Infect Dis 2018;18(1):43. https://doi.org/10.1186/s12879-018-2947-6.
8. Beig M, Ebrahimi E, Moradkasani S, Goodarzi F, Sholeh M, Golab N. Unravelling the challenge of cotrimoxazole and rifampin resistance in *B. melitensis* and *B. abortus*: A systematic review and meta-analysis. PLoS Negl Trop Dis 2024;18(12):e0012630. https://doi.org/10.1371/journal.pntd.0012630.
9. Beig M, Moradkasani S, Goodarzi F, Sholeh M. Prevalence of *Brucella melitensis* and *Brucella* abortus fluoroquinolones resistant isolates: A systematic review and meta-analysis. Vector-Borne Zoonotic Dis 2024;24(1):1 – 9. https://doi.org/10.1089/vbz.2023.0063.
10. Maduranga S, Valencia BM, Li XY, Moallemi S, Rodrigo C. A systematic review and meta-analysis of comparative clinical studies on antibiotic treatment of brucellosis. Sci Rep 2024;14(1):19037. https://doi.org/10.1038/s41598-024-69669-w.

Outbreak Reports

Early Detection and Response to the First Imported Case of Zika Virus Disease — Hainan Province, China, 2025

Xiangyu Yan[1,&]; Xiaoqing Fu[2,&]; Mingheng Wang[2]; Hao Yang[2]; Minghe Gu[3]; Jialin Liu[3]; Xianyi Zeng[2]; Qin Chen[2]; Lei Cui[4]; Xingqing Zhong[4]; Ling Zhang[4]; Jingjing Chen[4]; Yuming Jin[4]; Jian He[4]; Dapeng Yin[4]; Huiming Luo[4]; Tiejun Shui[5,#]; Yan Jin[4,#]

Summary

What is already known about this topic?

Zika virus (ZIKV) is primarily transmitted by *Aedes aegypti* and *Aedes albopictus*. The Zika epidemics in China were primarily imported cases.

What is added by this report?

This study documents the first laboratory-confirmed imported ZIKV case in Hainan Province, China. Phylogenetic analysis identified the Asian lineage, sharing 98.79% homology with a Thai strain.

What are the implications for public health practice?

This investigation highlighted the need to strengthen the patriotic health campaign, reducing local mosquito-borne transmission risk at the source. Multi-pathogen (dengue/chikungunya/Zika) testing of a single sample by Haikou Customs enabled Zika detection, while timely cross-department notification and coordinated response effectively enhanced outbreak containment.

ABSTRACT

Introduction: On September 2, 2025, a Singaporean national was reported Zika virus (ZIKV)-positive during inbound screening at Haikou Meilan Airport, Hainan Province, China. CDCs immediately launched epidemiological investigations, confirmatory laboratory testing, risk area delineation, and vector control measures.

Methods: Blood samples collected from the patient were tested for ZIKV nucleic acid using fluorescent quantitative polymerase chain reaction (PCR) technology. The complete viral genome sequence was obtained from the serum sample directly through a ZIKV-targeted sequencing with Oxford Nanopore. Phylogenetic analysis was conducted to determine the origin and genotype of the virus.

Results: Based on the patient's activity trajectory, the epidemic foci in Haikou City and Wenchang City were identified. The Breteau Indexes in the core areas were quickly reduced to below 5 within 5 days. Sequencing generated a 10,700-bp complete genome (ZIKA-HN/2025/China). Phylogenetic analysis revealed the Asian lineage, sharing 98.79% nucleotide homology with a Thailand strain (PP626399.1). No secondary cases were identified.

Conclusion: This imported case from Singapore was confirmed as the first ZIKV infection reported in Hainan Province. The climate and ecological conditions in Hainan required sustained suppression of mosquito density through source reduction under the patriotic health campaign. Multi-pathogen testing at ports, timely cross-department notification and coordination proved essential for early detection and effective containment.

On September 2, 2025, a Singaporean national of Chinese descent was reported Zika virus (ZIKV)-positive by Customs during inbound screening at Haikou Meilan Airport, Hainan Province, after arriving by air on September 1. Hainan CDC conducted epidemiological investigations, confirmatory testing, identified epidemic focus, and implemented health monitoring and mosquito vector control. Genetic sequencing revealed the ZIKV strain belonged to the Asian lineage. Timely control measures prevented local transmission.

INVESTIGATION AND RESULTS

On September 1, 2025, a 52-year-old male Singaporean national of Chinese descent traveled from Singapore to Haikou, entering through Haikou Meilan Airport at approximately 16:12. A whole blood sample was collected at the Customs and tested using the dengue-chikungunya-Zika triple assay kit with real-

Copyright © 2026 by Chinese Center for Disease Control and Prevention

time fluorescent PCR. At 15:30 on September 2, Customs notified Hainan Provincial CDC of a positive ZIKV nucleic acid result. Provincial CDC immediately deployed staff for investigation.

Epidemiological investigation showed the patient (a business owner) had no discomfort symptoms in the past month. Upon arrival, his temperature was 37.3 °C at screening and 37.4 °C on follow-up. On the afternoon of September 2, his temperature was 37.1 °C. He had no rash, joint pain, or conjunctivitis. No other passengers on the same flight showed ZIKV-related symptoms during routine screenings, so they did not receive testing or control measures.

During the two-day stay, his activities covered Haikou and Wenchang cities. On September 1, he returned directly to his cousin's home in Jinling Yaju Community, Longhua District, Haikou, and did not go out. At 8:51 on September 2, he had breakfast at Restaurant A, then drove to Wenchang. In Wenchang, his activity trajectory was as follows: from 10:30–10:50, he was at Wenchang Government Affairs Center; from 11:15–13:00, in his hometown in Nanpo Village; at 13:27, he had lunch at Restaurant B; at around 14:00, he returned to Haikou, arriving at his cousin's home at approximately 15:30, and did not go out again. He flew back to Singapore at 23:50 on September 3. No new cases emerged.

In terms of laboratory testing, provincial CDC re-tested the original sample, and reported ZIKV-positive [cycle threshold (Ct): 35] at 20:30 on September 2. Longhua District CDC re-collected his blood sample, and provincial CDC reported ZIKV-positive (Ct: 36) at 22:00. Detection was performed using fluorescent quantitative PCR (Jiangsu Bioperfectus kit, batch T202507013).

A 10,700-bp genome sequence was directly obtained from the serum sample (*ZIKA-HN/2025/China*) using Oxford Nanopore targeted sequencing for Zika (*1–4*). Basic Local Alignment Search Tool (BLAST) analysis showed 98.79% similarity to GenBank PP626399.1 (2017). Genetic evolution analysis showed that the virus belongs to the Asian lineage (Figure 1).

PUBLIC HEALTH RESPONSE

The patient was confirmed with ZIKV infection on the evening of September 2. Haiken Community Health Service Center in Longhua District reported the case as required. Municipal and district CDCs promptly conducted epidemiological investigations and delineated risk areas. The patient was guided to implement home-based quarantine with mosquito precautions because he planned to return to Singapore on September 3 and refused to go to medical institutions. The patient's residence was equipped with window screens, door screens, and mosquito nets, providing necessary conditions for home-based mosquito prevention and isolation. On September 3, under CDC guidance, he wore long clothing and boarded his flight back to Singapore (Figure 2A).

Provincial CDC conducted a rapid risk assessment. As a Class I dengue-endemic area nationally, Hainan has a climate similar to Southeast Asia, with higher *Aedes* density and wider distribution than other provincial-level administrative divisions (PLADs), posing greater localized transmission risk. Delayed or inadequate response could lead to secondary cases or wider outbreaks.

Based on the patient's activity trajectory, his residence building in Jinling Yaju Community in Haikou and Nanpo Village in Wenchang were designated as epidemic foci. A 200-meter radius from each epidemic focus was designated as the core zone, and an outer 200-meter radius as the alert zone. Because the patient spent short periods at the Government Affairs Center and the two restaurants, and not during the peak period of *Aedes* mosquito activity, these locations were not classified as epidemic foci but rather as risk sites. Health monitoring and education were strengthened in core zones, alert zones, risk sites, and other key sites (construction sites, urban villages, fringe areas), ensuring symptomatic individuals would promptly visit fever clinics. Medical institutions citywide enhanced surveillance and screening of febrile patients with suspected symptoms, emphasizing travel history to epidemic areas. Technical training for medical staff was strengthened to improve differential diagnosis of dengue, chikungunya, and Zika, as well as awareness of reporting. A multi-disease co-prevention approach was implemented to enhance surveillance sensitivity (Figure 2A).

For environmental vector control, rapid adult mosquito elimination and breeding site clearance were carried out in core zones, alert zones, and risk sites. Using the Breteau Index (BI) to monitor *Aedes* mosquito larvae and the human-baited double net trap method to monitor adult mosquitoes, emergency vector monitoring was conducted daily within core zones until mosquito density reached a safe level, then twice weekly until the outbreak ended. In core zones, adult mosquito density decreased to a safe level (0.9

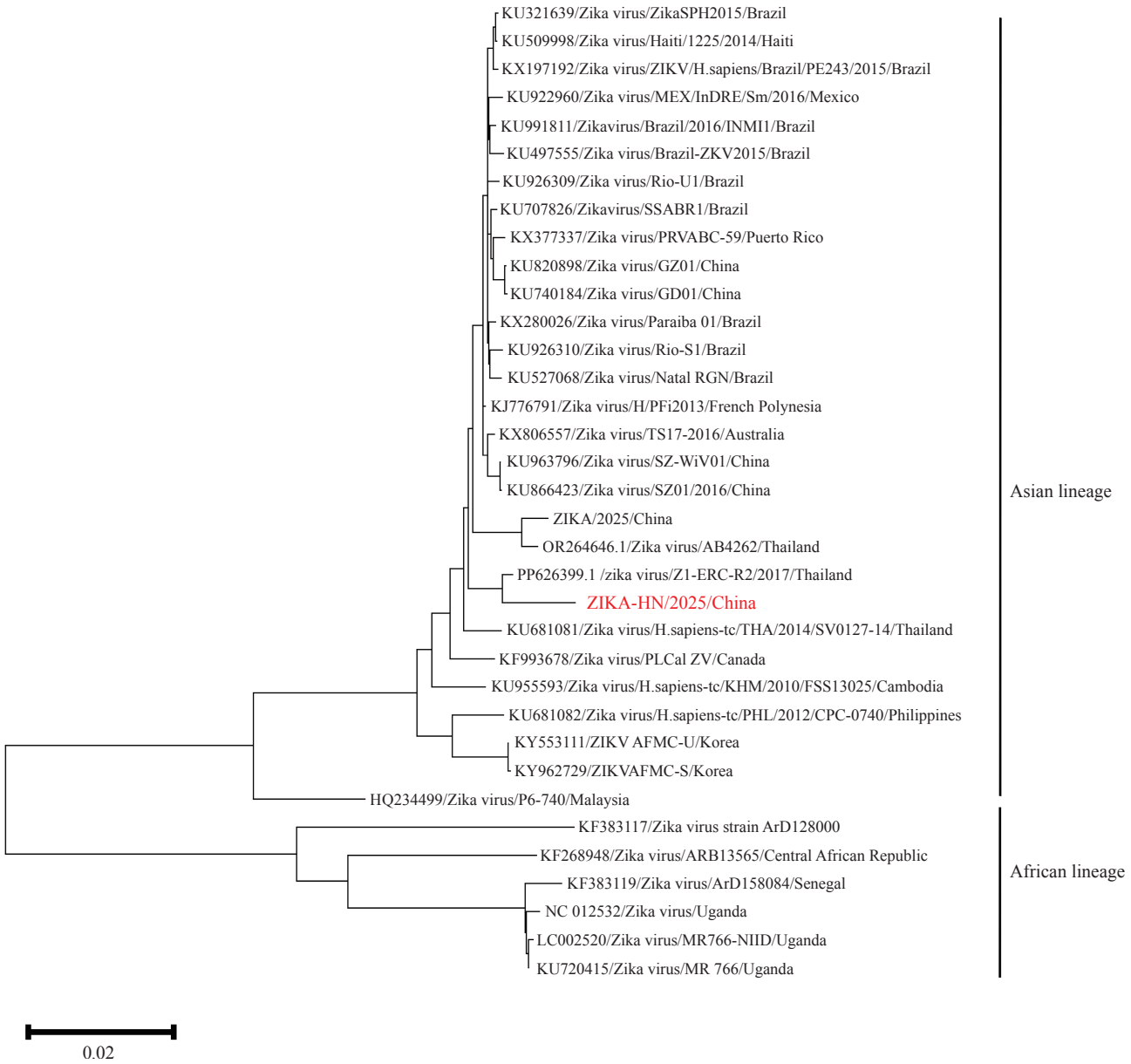

FIGURE 1. Phylogenetic tree of ZIKV whole-genome sequence.
Abbreviation: ZIKV=Zika virus.

per trap-hour) within 3 days. BI in Jinling Yaju Community was 5 on September 2, and 12 in Nanpo Village on September 3; both dropped below 5 within 5 days. Community staff mobilized residents for environmental sanitation improvements. Pest control operators received enhanced guidance and oversight. Municipal and district CDCs promptly fed back monitoring results and control recommendations to community staff to effectively guide epidemic prevention and control work. Mosquito-borne emergency monitoring continued for 24 consecutive days, with no secondary cases detected, and the outbreak was declared concluded (Figure 2A).

DISCUSSION

All ZIKV cases in China have been imported, with no local secondary transmission. The first imported case in Chinese mainland was reported in Jiangxi in February 2016 (*5*), followed by cases in Zhejiang, Guangdong, and other PLADs, showing a sporadic trend with main sources initially from South America (e.g., Venezuela) (*6*). As cross-border travel increased, the source shifted to Southeast Asia. Recently, Yunnan (2019) (*7*), Shandong (2025) (*8*), and Sichuan (2026) (*9*) reported imported cases from Myanmar, Thailand,

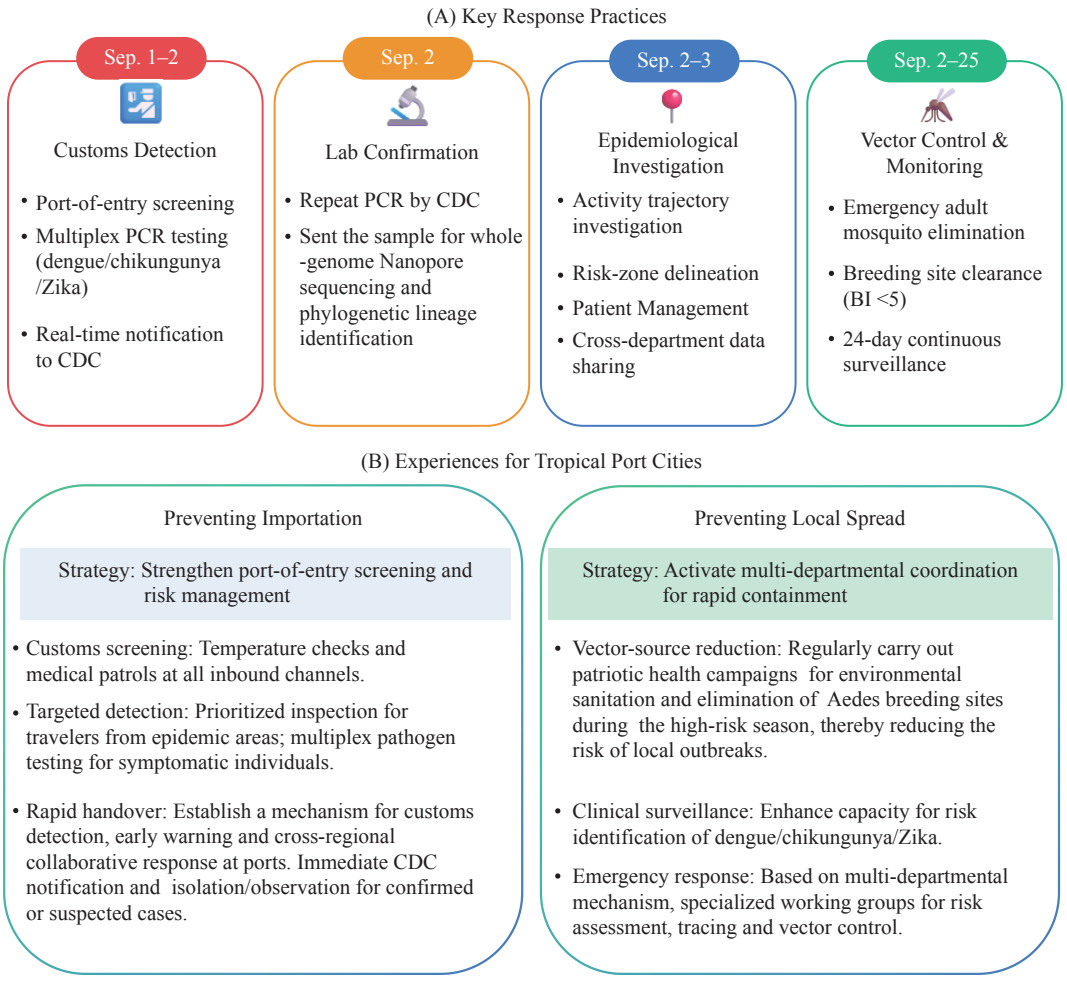

FIGURE 2. Key response practices and experiences for tropical port cities. (A) Key response practices. (B) Experiences for tropical port cities.
Abbreviation: BI=Breteau Index; PCR=polymerase chain reaction.

and Malaysia, respectively, with the Asian lineage predominating.

As Hainan's first ZIKV case, the case was imported from Singapore. Singapore experienced a minor Zika peak from 2023–2025 (30 cases in 2023, 13 in 2024, 16 in 2025) (*6*). In 2025, except one local case, most were imported from Southeast Asia (15 cases), explaining the strong homology between this study's virus sequence and the Thai strain (*10*). Compared with recent imported cases in Shandong (*8*) and Sichuan (*9*), despite different countries of origin, all sequences showed strong homology with the Thai strain, indicating the primary importation risk source and priorities for pathogen surveillance.

The epidemic control provided a model for multiplex pathogen joint testing and coordinated emergency management in tropical ports and other high-risk border areas (Figure 2B). The patient in Hainan had an insidious onset with inconspicuous symptoms, posing risk of cryptic transmission and local spread. Therefore, disease surveillance awareness and timely result notification of Meilan Airport Customs were crucial for early detection. Multiplex nucleic acid testing with different fluorescent dyes enabled simultaneous detection of multiple targets, reducing laboratory workload and turnaround time versus single-target assays. Furthermore, the multi-departmental coordination mechanism was also important. After the outbreak, Haikou activated its emergency response mechanism, established an on-site command center, and launched a joint epidemiological investigation by public security, public health, and information technology teams. Seven task forces — information, patriotic health and disinfection, environmental improvement, household screening, environmental monitoring, source tracing, and supervision and education — ensured seamless operation. To build a second defense line beyond the

border, stronger international epidemic intelligence and risk assessment, closer Customs coordination, screening of inbound travelers from key areas, and post-entry health monitoring are essential.

Successful containment of this imported epidemic also benefited from timely emergency response measures, including scientifically defining risk zones, classified and graded epidemic management, and emergency vector mosquito monitoring and control. Since 2024, Hainan has conducted a three-year patriotic health special campaign, implemented ledger management of mosquito breeding sites and carry out breeding site inspections, dynamically clearing mosquito breeding grounds. Continuously suppressing *Aedes* vector density during the high-risk season for mosquito-borne infectious diseases and reducing the risk of local outbreaks can provide practical reference for other PLADs in China that face the risk of local mosquito-borne diseases transmission (Figure 2B). Since the Hainan Free Trade Port closed its customs operations on December 18, 2025, economic, trade, and personnel exchanges with Southeast Asian countries have become increasingly frequent, raising the risk of importing mosquito-borne infectious diseases. Therefore, multiplex pathogen testing for strengthening port-of-entry detection, and multi-departmental coordination mechanism for rapid containment should remain a long-term priority.

Conflicts of interest: No conflicts of interest.

Ethical statement: Approval by the Ethics Committee of Hainan Center for Disease Control and Prevention, China (approval number: 2025005).

Acknowledgements: Supported by Hainan Provincial Natural Science Foundation of China (326MS0423), and National Natural Science Foundation of China (72604287).

doi: 10.46234/ccdcw2026.201

[#] Corresponding authors: Tiejun Shui, shuitiejunynjkedu@163.com; Yan Jin, jinyanfangyi@sina.com.

[1] School of Disaster and Emergency Medicine, Tianjin University, Tianjin, China; [2] Haikou Center for Disease Control and Prevention, Haikou City, Hainan Province, China; [3] School of Medicine, Tianjin University, Tianjin, China; [4] Hainan Provincial Center for Disease Control and Prevention (Hainan Academy of Preventive Medicine), Haikou City, Hainan Province, China; [5] Yunnan Center for Disease Control and Prevention, Kunming City, Yunnan Province, China.
[&] Joint first authors.

Copyright © 2026 by Chinese Center for Disease Control and Prevention & Chinese Academy of Preventive Medicine. All content is distributed under a Creative Commons Attribution Non Commercial License 4.0 (CC BY-NC).

Submitted: June 28, 2026
Accepted: September 25, 2026
Issued: October 02, 2026

REFERENCES

1. Gu SH, Song DH, Lee D, Jang J, Kim MY, Jung J, et al. Whole-genome sequence analysis of Zika virus, amplified from urine of traveler from the Philippines. Virus Genes 2017;53(6):918 – 21. https://doi.org/10.1007/s11262-017-1500-9.
2. Khongwichit S, Chuchaona W, Vongpunsawad S, Poovorawan Y. Molecular epidemiology, clinical analysis, and genetic characterization of Zika virus infections in Thailand (2020-2023). Sci Rep 2023;13(1):21030. https://doi.org/10.1038/s41598-023-48508-4.
3. Rajaiah P, Gupta B, Mayilsamy M. ZIKA virus, an emerging arbovirus in India: a glimpse of global genetic lineages. Microorganisms 2025;13(3):544. https://doi.org/10.3390/microorganisms13030544.
4. Zadra N, Rizzoli A, Rota-Stabelli O. Comprehensive phylogenomic analysis of Zika virus: insights into its origin, past evolutionary dynamics, and global spread. Virus Res 2024;350:199490. https://doi.org/10.1016/j.virusres.2024.199490.
5. Liao Y, Zeng ZL, Hu GL, Yang JP, Yuan H, Li JH, et al. Survey of the first case of Zika virus disease in the mainland of China. Chin J Epidemiol 2016;37(5):593 – 6. https://doi.org/10.3760/cma.j.issn.0254-6450.2016.05.001.
6. Wang YL, Zhang XY, Ren RQ, Li C, Xiang NJ, Tu WX, et al. Epidemiological and clinical characteristics of 25 imported Zika cases in mainland China. Chin J Vector Biol Control 2017;28(6):535 – 7. https://doi.org/10.11853/j.issn.1003.8280.2017.06.005.
7. Zhao DN, Li HC, Zhang HJ, Shi J, Guo JW, Yang L, et al. Dengue virus, chikungunya virus, and Zika virus infections in febrile cases in Gengma county, Yunnan province, in 2019. Dis Surveill 2024;39(6):711 – 7. https://doi.org/10.3784/jbjc.202305040194.
8. Zhang S, Wu JL, Wang D, Song JD, Li Y, Yin CH, et al. The first imported case of Zika virus infection - Shandong Province, China, 2025. China CDC Wkly 2025;7(30):1004 – 8. https://doi.org/10.46234/ccdcw2025.169.
9. Hu LW, Tian LB, Yan K, Zhang S, Xie WJ, Feng J, et al. An imported case of dengue/Zika coinfection - Sichuan Province, China, 2026. China CDC Wkly 2026;8(13):394 – 8. https://doi.org/10.46234/ccdcw2026.063.
10. Communicable Diseases Agency. Weekly infectious diseases bulletin 2025. 2026. https://www.cda.gov.sg/resources/weekly-infectious-diseases-bulletin-2025/. [2026-1-8].

Outbreak Reports

A Cluster of Haff Disease Associated with Consumption of *Cyprinus carpio rubrofuscus* — Heyuan City, Guangdong Province, China, 2026

Lingling Lu[1,&]; Weiguang Luo[2,&]; Huiming Guo[2]; Yulin Chen[2]; Wenxiu Ye[2]; Peidi Luo[2]; Pingmei Huang[2]; Jian Wen[1]; Qiong Huang[1,#]

Summary

What is already known about this topic?

Haff disease is a foodborne rhabdomyolysis syndrome. In China, most reported cases are associated with crayfish, whereas freshwater fish-associated cases are rare, with only two previously documented clusters.

What is added by this report?

This cluster confirmed *Cyprinus carpio rubrofuscus* (red-tailed carp) as a Haff disease vector, representing the second carp-associated cluster in China and the first from the Dongjiang River Basin. All five consumers of cooked carp developed rhabdomyolysis (attack rate: 100%, 5/5; Fisher's exact test, P=0.0079), whereas the two non-consumers remained healthy, indicating that the unidentified causative factor was heat-stable.

What are the implications for public health practice?

Clinicians evaluating patients with unexplained rhabdomyolysis should routinely ask about recent consumption of aquatic products. Local health authorities should include wild-caught freshwater fish in risk communication.

ABSTRACT

Introduction: Haff disease is a rare foodborne rhabdomyolysis syndrome with only scattered reports linked to freshwater fish in China.

Methods: On April 25, 2026, a cluster of five suspected Haff disease cases following a family dinner was reported to Longchuan County Center for disease control and prevention in Heyuan City, Guangdong Province. Epidemiological investigation was conducted.

Results: Among the seven diners, five met the criteria for suspected cases (four were confirmed). All five patients had consumed *Cyprinus carpio rubrofuscus* (attack rate: 100%, 5/5); two non-consumers remained healthy (Fisher's exact test, P=0.0079). The median incubation period was 11.3 hours (range: 4.2–13.2 hours). All patients recovered after symptomatic treatment. The illness occurred after the consumption of cooked carp, indicating that the unidentified causative factor was heat-stable.

Conclusion: This is the second documented carp-associated Haff disease cluster in China, and the first from the Dongjiang River Basin. These findings suggest that clinicians should consider a detailed dietary history of aquatic product consumption when evaluating unexplained rhabdomyolysis.

Haff disease involves unexplained rhabdomyolysis that occurs within 24 h of eating certain seafood, especially fish (*1*–*2*). The typical symptoms include muscle pain and markedly elevated serum creatine kinase (CK) levels. Internationally, the associated fish species include burbots, buffalo fish (*Ictiobus cyprinellus*), and freshwater pomfrets (*1*). In China, most cases have been linked to crayfish (*Procambarus clarkii*) (*3*), with only two documented clusters of freshwater fish: a carp cluster in Guangxi Zhuang Autonomous Region (*4*) and a freshwater pomfret outbreak in Guangdong Province (*5*). This report describes a cluster of Haff disease cases linked to the consumption of *Cyprinus carpio rubrofuscus* (*6*), locally known as red-tailed carp, in Longchuan County, Heyuan City, Guangdong Province, in April 2026.

INVESTIGATION AND RESULTS

Cluster Detection

On April 25, 2026, at 17:30, a local hospital in Longchuan County reported that five villagers from a town presented with vomiting, abdominal pain, and limb soreness after a family dinner on April 24.

Copyright © 2026 by Chinese Center for Disease Control and Prevention

Laboratory tests revealed elevated CK and creatine kinase-MB (CK-MB) levels.

Case Definitions

Case definitions were adapted from previous Haff disease investigations (*2,7*).

Suspected case Any person who dined with an affected family member on April 24 and subsequently developed unexplained muscle pain, vomiting, or diarrhea.

Clinically confirmed case A suspected case with serum CK levels exceeding 5 times the upper limit of normal (ULN; >950 U/L, based on a local reference range of 190 U/L).

Epidemiological Features

The cluster involved five cases from an extended family that, together with two other people, shared dinner at approximately 20:30 on April 24; no other meals were shared. The first case occurred at 00:40 on April 25 and the last at 09:40, consistent with point-source exposure. The median incubation period was 11.3 hours (range: 4.2–13.2 hours). The patients ranged in age from 35 to 69 years (three males and two females). All five patients and the fishermen reported normal daily labor activities with no history of strenuous exercise or muscle trauma 3 days before symptom onset.

Clinical Characteristics

Five suspected cases were identified (attack rate: 100%, 5/5), and four met the clinically confirmation criteria. Common symptoms of suspected cases included myalgia (100%, 5/5), vomiting (80%, 4/5), chest tightness (60%, 3/5), abdominal pain (40%, 2/5), and diarrhea (20%, 1/5); no cases presented with dark urine. The CK levels ranged from 1,181.2 to 12,428.2 U/L (6–65 × ULN). The CK-MB levels ranged from 37.5 to 926.3 U/L. All patients recovered after three to eight days of supportive treatment.

Food Exposure Investigation

The implicated meal included chicken, vegetables, fried tofu, shrimp, and an approximately 2.5-kg wild carp given by a friend who caught it in a small inlet of a local reservoir earlier that day. Two preparation methods were used for carp: 1) Raw carp fillets ("Yu Sheng") — sliced raw flesh; 2) Cooked carp parts — steamed mixture of bones, tail, head, skin, and roe.

Of the seven diners, five consumed carp (three ate both raw and cooked portions; two ate only cooked portions), and all ate chicken, vegetables, fried tofu, and shrimp. Four of the five carp consumers drank homemade jujube wine during their meals. None of the unaffected individuals consumed carp. Notably, the friend who caught the carp, along with another fisherman, consumed two smaller carp (approximately 500–1,000 g each) and several tilapia from the same location on the same day without becoming ill. Photographic identification confirmed the fish to be *Cyprinus carpio rubrofuscus*, locally known as red-tailed carp, and confirmed the shrimp to be the East Asian River prawn, *Macrobrachium nipponense.*

Statistical Analysis

An epidemiological investigation was conducted among the seven diners (Table 1). Carp consumption was strongly associated with illness; all five consumers developed Haff disease compared with neither of the two non-consumers (Fisher's exact test, two-sided P=0.0079). The relative risk could not be calculated because of zero events among non-consumers. All five cases consumed cooked carp, and three cases additionally consumed raw carp fillets; all consumers developed illness regardless of the preparation method.

Environmental Investigation

Carp were harvested from the secluded inlet of a

TABLE 1. A cluster of suspected Haff disease associated with consumption of *Cyprinus carpio rubrofuscus* among ill and well co-diners — Heyuan City, Guangdong Province, April 2026.

Exposure	No. of exposed	No. of ill	Attack rate (%)
Did not consume any carp	2	0	0
Consumed any carp	5	5	100
Consumed raw carp fillets only	0	0	0
Consumed cooked carp parts only	2	2	100
Consumed both raw carp fillets and cooked carp parts	3	3	100
Total diners	7	5	71

local reservoir. The water was clear.

Public Health Response

Following confirmation of the cluster, the local County Center for Disease Control and Prevention (CDC) promptly notified local hospitals to consider Haff disease in patients with rhabdomyolysis and to obtain detailed exposure information, including a 3-day retrospective dietary history, drinking water history, physical activity, and occurrence of infectious illness. In addition, the prefecture-level CDC conducted a case search through the Foodborne Disease Surveillance System from April 24 to 26 and found no other patients with similar symptoms or a history of consuming the same fish in the city. The county government advised residents to avoid eating wild-caught carp from the local reservoir inlet during the ongoing investigation.

DISCUSSION

This cluster met the established criteria for Haff disease (*2*,*7*): 1) onset of rhabdomyolysis within 24 h of fish consumption; 2) similar clinical symptoms among co-exposed individuals; 3) all individuals who ate the carp became sick (100% attack rate); and 4) exclusion of other food items (chicken, vegetables, tofu, and shrimp) as potential causes.

All five patients ate cooked carp, whereas the non-consumers remained healthy. This suggests that cooking did not eliminate the unidentified causative factors, consistent with earlier reports on Haff disease (*2*). The fisherman who ate the smaller *Cyprinus carpio rubrofuscus* from the same waters did not become ill, whereas all consumers of the approximately 2.5-kg carp became ill. Whether fish size influenced illness could not be determined from this cluster alone, and because the smaller fish were completely consumed, the triggering substances could not be compared between them. Strenuous exercise is a recognized trigger of rhabdomyolysis (*8*); however, all five cases and the fishermen reported only routine daily labor in the three days before they got sick, so exercise is unlikely to have contributed to illness in this cluster.

The principal contribution of this cluster was the confirmation of *Cyprinus carpio rubrofuscus* (red-tailed carp) as an additional vector of Haff disease, with the first report from the Dongjiang River basin. This suggests that freshwater fish other than crayfish may be an underestimated source of Haff disease in South China. The cause of Haff disease has remained unidentified for nearly a century (*1*). We retained leftover fish samples, which could be tested in the future using non-targeted metabolomics.

This cluster had only five cases; therefore, we could not perform dose–response or subgroup analyses. In addition, the carp were prepared using two methods (raw fillets and cooked parts, including roe), so we could not determine whether roe or other parts of the fish caused the illness.

When evaluating unexplained rhabdomyolysis, clinicians should obtain a thorough dietary history of aquatic products regardless of cooking method (*1*,*9*). Haff disease surveillance in the region should include freshwater fish, rather than focusing solely on crayfish. Public health messages are needed to warn residents of the risks of consuming wild-caught freshwater fish. Further research on the environmental and chemical triggers of Haff disease in freshwater ecosystems of China is important.

Ethical statement: Ethical review and approval were not required for this investigation, as it was conducted as part of routine public health emergency response activities under the Food Safety Law of the People's Republic of China on the Prevention and Treatment of Foodborne Diseases.

Conflicts of interest: None declared.

doi: 10.46234/ccdcw2026.202

[#] Corresponding author: Qiong Huang, huangqiong@cdcp.org.cn.

[1] Guangdong Provincial Center for Disease Control and Prevention, Guangzhou City, Guangdong Province, China; [2] Longchuan County Center for Disease Control and Prevention, Heyuan City, Guangdong Province, China.
[&] Joint first authors.

Copyright © 2026 by Chinese Center for Disease Control and Prevention & Chinese Academy of Preventive Medicine. All content is distributed under a Creative Commons Attribution Non Commercial License 4.0 (CC BY-NC).

Submitted: July 17, 2026
Accepted: September 12, 2026
Issued: October 02, 2026

REFERENCES

1. Pei P, Li XY, Lu SS, Liu Z, Wang R, Lu XC, et al. The emergence, epidemiology, and etiology of Haff disease. Biomed Environ Sci 2019;32 (10):769 – 78. https://doi.org/10.3967/bes2019.096.
2. Buchholz U, Mouzin E, Dickey R, Moolenaar R, Sass N, Mascola L. Haff disease: from the Baltic Sea to the U. S. shore. Emerg Infect Dis 2000;6(2):192 – 5. https://doi.org/10.3201/eid0602.000215.
3. Xu FY, Guo CH, Wang Y, Zhu Y. Outbreak of Haff disease caused by crayfish in China: a systematic review. J Health Popul Nutr 2024;43(1): 195. https://doi.org/10.1186/s41043-024-00682-5.

4. Zeng JS, Liu YP, Ma HL, Liu HH, Li YH, Mo SL, et al. A cluster of rhabdomyolysis syndrome resulting from carp consumption in Gongcheng Yao Autonomous County, Guangxi, 2016. China CDC Wkly 2020;2(2):25 – 7. https://doi.org/10.46234/ccdcw2020.006.
5. Huang X, Li YP, Huang Q, Liang JH, Liang CS, Chen BF, et al. A past Haff disease outbreak associated with eating freshwater pomfret in South China. BMC Public Health 2013;13:447. https://doi.org/10.1186/1471-2458-13-447.
6. Zheng CY. Fishes of Pearl river. Beijing: Science Press. 1989; p. 226-33. https://book.kongfz.com/15621/7437037568. (In Chinese).
7. Centers for Disease Control and Prevention (CDC). Haff disease associated with eating buffalo fish-United States, 1997. MMWR Morb Mortal Wkly Rep 1998;47(50):1091-93. https://pubmed.ncbi.nlm.nih.gov/9883771/.
8. Kim J, Lee J, Kim S, Ryu HY, Cha KS, Sung DJ. Exercise-induced rhabdomyolysis mechanisms and prevention: a literature review. J Sport Health Sci 2016;5(3):324 – 33. https://doi.org/10.1016/j.jshs.2015.01.012.
9. Chan TYK. The emergence and epidemiology of Haff disease in China. Toxins (Basel) 2016;8(12):359. https://doi.org/10.3390/toxins8120359.

Notifiable Infectious Diseases Reports

Reported Cases and Deaths of National Notifiable Infectious Diseases — China, July 2026*

Diseases	Cases	Deaths
Plague	0	0
Cholera	4	0
COVID-19	521,751	1
SARS-CoV	0	0
Acquired immune deficiency syndrome†	4,086	1,526
Hepatitis	147,945	284
Hepatitis A	1,638	0
Hepatitis B	126,727	34
Hepatitis C	15,974	249
Hepatitis D	25	0
Hepatitis E	2,836	1
Other hepatitis	745	0
Poliomyelitis	0	0
Human infection with noval influenza virus	8	0
Measles	60	0
Epidemic hemorrhagic fever	258	0
Rabies	35	37
Japanese encephalitis	19	2
Dengue	1,120	0
Monkey pox§	83	0
Chikungunya fever	186	0
Severe fever with thrombocytopenia syndrome	978	58
Anthrax	79	1
Dysentery	3,438	0
Tuberculosis	58,871	190
Typhoid fever and paratyphoid fever	467	0
Meningococcal meningitis	18	0
Pertussis	616	0
Diphtheria	1	0
Neonatal tetanus	2	0
Scarlet fever	1,763	0
Brucellosis	6,996	2
Gonorrhea	13,411	0
Syphilis	58,058	2
Leptospirosis	100	0
Schistosomiasis	1	0
Malaria	523	1

Copyright © 2026 by Chinese Center for Disease Control and Prevention

Continued

Diseases	Cases	Deaths
Influenza	969,125	3
Mumps	5,818	0
Rubella	31	0
Acute hemorrhagic conjunctivitis	1,589	0
Leprosy	22	0
Typhus	132	0
Kala azar	35	0
Echinococcosis	952	0
Filariasis	0	0
Hand, foot and mouth disease	206,564	0
Infectious diarrhea[¶]	145,175	0
Total	2,150,320	2,107

* According to the National Bureau of Disease Control and Prevention.
[†] The number of deaths of Acquired immune deficiency syndrome (AIDS) is the number of all-cause deaths reported in the month by cumulative reported AIDS patients.
[§] Since September 20, 2023, Monkey pox was included in the management of Class B infectious diseases.
[¶] Infectious diarrhea excludes cholera, dysentery, typhoid fever and paratyphoid fever.
The number of cases and cause-specific deaths refer to data recorded in National Notifiable Disease Reporting System in China, which includes both clinically-diagnosed cases and laboratory-confirmed cases. Only reported cases of the 31 provincial-level administrative divisions in the Chinese mainland are included in the table, whereas data of Hong Kong Special Administrative Region, Macau Special Administrative Region, and Taiwan, China are not included. Monthly statistics are calculated without annual verification, which were usually conducted in February of the next year for de-duplication and verification of reported cases in annual statistics. Therefore, 12-month cases could not be added together directly to calculate the cumulative cases because the individual information might be verified via National Notifiable Disease Reporting System according to information verification or field investigations by local CDCs.

doi: 10.46234/ccdcw2026.203

Copyright © 2026 by Chinese Center for Disease Control and Prevention & Chinese Academy of Preventive Medicine. All content is distributed under a Creative Commons Attribution Non Commercial License 4.0 (CC BY-NC).

Submitted: August 21, 2026
Accepted: September 07, 2026
Issued: October 02, 2026

Youth Editorial Board

Director Lei Zhou

Vice Directors Jue Liu Tiantian Li Tianmu Chen

Members of Youth Editorial Board

Jingwen Ai
Liangliang Cui
Jia Huang
Min Kang
Fangfang Li
Jun Liu
Yang Pan
Shuhui Song
Jingyuan Wang
Xin Wang
Meng Xiao
Lin Yang
Yang Zhao
Li Bai
Meng Gao
Xiang Huo
Huihui Kong
Jingxin Li
Li Liu
Zhixing Peng
Kun Su
Linghang Wang
Feixue Wei
Tian Xiao
Canqing Yu
Hong Zhou
Yuhai Bi
Jie Gong
Xiaolin Jiang
Lingcai Kong
Huigang Liang
Yang Liu
Menbao Qian
Song Tang
Qihui Wang
Yongyue Wei
Wuxiang Xie
Lin Zeng
Yunlong Cao
Yuehua Hu
Yu Ju
Shengjie Lai
Di Liu
Chao Ma
Tian Qin
Bin Wang
Xiaoli Wang
Zhiqiang Wu
Lei Xu
Yi Zhang

Indexed by Science Citation Index Expanded (SCIE), Social Sciences Citation Index (SSCI), PubMed Central (PMC), Scopus, Chinese Scientific and Technical Papers and Citations, and Chinese Science Citation Database (CSCD)

Copyright © 2026 by Chinese Center for Disease Control and Prevention & Chinese Academy of Preventive Medicine

Under the terms of the Creative Commons Attribution-Non Commercial License 4.0 (CC BY-NC), it is permissible to download, share, remix, transform, and build upon the work provided it is properly cited. The work cannot be used commercially without permission from the journal.

References to non-China-CDC sites on the Internet are provided as a service to *CCDC Weekly* readers and do not constitute or imply endorsement of these organizations or their programs by China CDC or National Health Commission of the People's Republic of China. China CDC is not responsible for the content of non-China-CDC sites.

The inauguration of *China CDC Weekly* is in part supported by Project for Enhancing International Impact of China STM Journals Category D (PIIJ2-D-04-(2018)) of China Association for Science and Technology (CAST).

CHINA CDC WEEKLY

CCDC weekly

Vol. 8 No. 40 Oct. 2, 2026

中国疾病预防控制中心周报(英文)

Responsible Authority
National Disease Control and Prevention Administration

Sponsor
Chinese Center for Disease Control and Prevention &
Chinese Academy of Preventive Medicine

Editor-in-Chief
Jianwei Wang

Editing and Publishing
China CDC Weekly Editorial Office
No.155 Changbai Road, Changping District, Beijing, China
Tel: 86-10-63150501, 63150701
Email: weekly@chinacdc.cn

Printing: Beijing Kexin Printing Co., Ltd

Complimentary Access

CSSN
ISSN 2096-7071 (Print)
ISSN 2097-3101 (Online)
CN 10-1629/R1